Math. Proc. Camb. Phil. Soc. (2026), **180**, 275–301
doi:10.1017/S0305004125101746
First published online 16 October 2025

Infinitely many standard trisection diagrams for Gluck twisting

BY TSUKASA ISOSHIMA
Research and Education Center for Natural Sciences, Keio University, 4-1-1 *Hiyoshi, Kohoku-ku, Yokohama, Kanagawa,* 223-8521, *Japan.*
e-mail: isoshima@keio.jp

(*Received* 03 *January* 2024*; revised* 13 *June* 2025*; accepted* 04 *August* 2025)

Abstract

Gay and Meier asked if a trisection diagram for the Gluck twist on a spun or twist-spun 2-knot in S^4 obtained by a certain method is standard. In this paper, we show that the trisection diagram for the Gluck twist on the spun $(p+1, p)$-torus knot is standard, where p is any integer greater than or equal to 2.

2020 Mathematics Subject Classification: 57K40 (Primary);
57R65 (Secondary)

1. *Introduction*

A trisection, which was introduced by Gay and Kirby [**5**], is roughly a decomposition of a closed oriented smooth 4-manifold into three 4-dimensional 1-handlebodies, namely, the union of a 0-handle and 1-handles. A trisection is a 4-dimensional analogue of a Heegaard splitting, a well known decomposition of a 3-manifold into two 3-dimensional 1-handlebodies. Just as the decomposition of a Heegaard splitting is described by a Heegaard diagram, the decomposition of a trisection is described by a trisection diagram. A trisection diagram is a 4-tuple which consists of a closed oriented surface appearing as the triple intersection of components of the decomposition and three families of simple closed curves α, β and γ in the surface. There is a one-to-one correspondence between trisections and trisection diagrams under an appropriate equivalence relation. A trisection diagram recovers a handle decomposition of the 4-manifold by taking the product of a 2-dimensional disk to the surface and attaching 2-handles along the α, β and γ curves with the surface framings.

It is shown as a corollary from the existence and uniqueness of trisections up to stabilisation that two closed 4-manifolds are diffeomorphic if and only if two corresponding trisection diagrams are related by surface diffeomorphisms, handle slides among the same family curves and stabilisations. However, given two trisection diagrams of the same 4-manifold with the same type (see Definition 2·2 for the type of a trisection diagram), it is generally difficult to decide whether stabilisations are necessary or not. Here, let us recall examples where stabilisations are required and where they are not. As an example of the former case, Islambouli [**9**] showed that there exist spun Seifert fibered spaces that admit non-isotopic trisections with the same type. Namely, trisection diagrams corresponding to these 4-manifolds cannot be related to each other without stabilisations. As an example of

© The Author(s), 2025. Published by Cambridge University Press on behalf of Cambridge Philosophical Society.

https://doi.org/10.1017/S0305004125101746 Published online by Cambridge University Press

the latter case, it is easy to check that the two (2,0)-trisection diagrams of $\mathbb{C}P^2\#\overline{\mathbb{C}P^2}$ and $S^2\tilde{\times}S^2$, the non-trivial sphere bundle over the sphere, depicted in [5], are related without stabilisations. With respect to S^4, it is conjectured, called the 4-dimensional Waldhausen conjecture, that each trisection of S^4 is isotopic to the genus-0 trisection or its stabilisation [15]. In terms of trisection diagrams, the 4-dimensional Waldhausen conjecture asserts that each trisection diagram $\mathcal{D}$ of S^4 is related to the stabilisation of the genus-0 trisection diagram, whose type is the same as the type of $\mathcal{D}$, without stabilisations. Actually, there is some supporting evidence of the conjecture (for example, [10, 15]. However, this conjecture is believed to be false at present by [15], and there are some potential counterexamples. In this paper, we explore one family of potential counterexamples coming from trisections of Gluck twisted 4-manifolds that are diffeomorphic to S^4.

The Gluck twist is a cutting and pasting operation on a 2-knot. Let X be a closed 4-manifold and K be a 2-knot in X with normal Euler number 0. Then, the Gluck twisted 4-manifold $\Sigma_K(X) = X - \mathrm{int}(\nu(K)) \cup_\tau S^2 \times D^2$, where τ is the non-trivial self-diffeomorphism of $S^2 \times S^1$ defined by $\tau(z, e^{i\theta}) = (ze^{i\theta}, e^{i\theta})$, and $\nu(K)$ is a tubular neighbourhood of K in X. If $X = S^4$, the Gluck twisted 4-manifold on any 2-knot is a homotopy 4-sphere [7], and hence homeomorphic to S^4 by Freedman's theorem [4]. Moreover, it is well known that $\Sigma_K(S^4)$ is diffeomorphic to S^4 if K is a spun 2-knot or twist-spun 2-knot [7, 8]. Thus, a corresponding trisection diagram and the stabilisation of the genus-0 trisection diagram are related by the three operations including stabilisations. However, it is not known if the resulting trisection diagram can be destabilised some number of times to get the genus-0 trisection diagram, or if stabilisations are required. Then, Gay and Meier asked the following question:

Question 1·1 ([6]). Let $\mathcal{K}$ be the spin or the twist-spin of a non-trivial knot K in S^3. Is a trisection diagram of $\Sigma_{\mathcal{K}}(S^4)$ constructed from a doubly-pointed Heegaard diagram of K by combining some methods **ever** standard?

Note that we say that a trisection diagram of a 4-manifold that is diffeomorphic to S^4 is *standard* if it is the stabilisation of the genus-0 trisection diagram after surface diffeomorphisms and handle slides.

The first answer to Question 1·1 was obtained in [11, theorem 1·1], in which the author and Ogawa showed that in Question 1·1, if we take the trefoil knot as the 1-knot K and take Figure 3 as its doubly-pointed Heegaard diagram, then the trisection diagram of $\Sigma_{\mathcal{K}}(S^4)$ in Question 1·1 is standard.

Let $\mathcal{D}_p$ be the trisection diagram of $\Sigma_{S(T(p+1,p))}(S^4)$ in Question 1·1 obtained by taking the $(p+1, p)$-torus knot $T(p+1, p)$ as the 1-knot K and taking Figure 3 as its doubly-pointed Heegaard diagram, where $S(T(p+1, p))$ is the spun $(p+1, p)$-torus knot. The trisection diagram $\mathcal{D}_p$ is shown explicitly in Figure 15. In this paper, we show the following main theorem.

THEOREM (Theorem 4·1). *The trisection diagram $\mathcal{D}_p$ ($p \geq 2$) is standard.*

Note that [11, theorem 1·1] corresponds to the case of $p = 2$ in the main theorem. The proof of the theorem requires a large number of Dehn twists and handle slides, as well as an inductive argument we call the seesaw lemma (Lemma 4·6).

Organisations. We briefly review preliminaries, specifically (relative) trisections of 4-manifolds (with boundary) and doubly pointed Heegaard/trisection diagrams in Section 2.

https://doi.org/10.1017/S0305004125101746 Published online by Cambridge University Press

In Section 3, we construct the trisection diagram in the question for the spun $(p+1,p)$-torus knot explicitly by the methods mentioned in the question. Then we prove the main theorem in Section 4. We have further remarks in Section 5.

2. *Preliminaries*

In this section, we review notions used in Section 3 and 4. In this paper, unless otherwise stated, any 4-manifold is compact, connected, oriented and smooth, and any surface-knot is a connected, closed surface smoothly embedded in a 4-manifold.

2·1. *Trisections and relative trisections*

In this subsection, we recall (relative) trisections of 4-manifolds (with boundary).

Definition 2·1. Let X be a closed 4-manifold. A $(g;k_1,k_2,k_3)$-*trisection* of X is a 3-tuple (X_1,X_2,X_3) satisfying the following conditions:

(i) $X=X_1\cup X_2\cup X_3$;
(ii) for each $i=1,2,3$, $X_i\cong \natural_{k_i} S^1\times D^3$;
(iii) for each $i=1,2,3$, $X_i\cap X_j\cong \natural_g S^1\times D^2$;
(iv) $X_1\cap X_2\cap X_3\cong \#_g S^1\times S^1=\Sigma_g$.

Note that g and k_i are non-negative integers with $k_i\leq g$ for each i. Let $H_\alpha=X_3\cap X_1$, $H_\beta=X_1\cap X_2$ and $H_\gamma=X_2\cap X_3$. The union $H_\alpha\cup H_\beta\cup H_\gamma$ is called the *spine* of the trisection. A trisection is uniquely determined by its spine. The 4-tuple of non-negative integers $(g;k_1,k_2,k_3)$ is called the *type* of the trisection. Note that if $k_1=k_2=k_3$, the trisection is said to be *balanced*, and the type is denoted by (g,k) for short, where $k=k_i$ $(i=1,2,3)$. Each X_i is called a *sector*.

The decomposition of a trisection is described by a trisection diagram.

Definition 2·2. A 4-tuple $(\Sigma_g,\alpha,\beta,\gamma)$ is called a $(g;k_1,k_2,k_3)$-*trisection diagram* if the following holds:

(i) (Σ_g,α,β) is a Heegaard diagram of $\#_{k_1} S^1\times S^2$;
(ii) (Σ_g,β,γ) is a Heegaard diagram of $\#_{k_2} S^1\times S^2$;
(iii) (Σ_g,γ,α) is a Heegaard diagram of $\#_{k_3} S^1\times S^2$.

Similar to the type of a trisection, the 4-tuple of non-negative integers $(g;k_1,k_2,k_3)$ is called the *type* of the trisection diagram.

Definition 2·3. A *stabilisation* of a trisection diagram is the connected-sum of the trisection diagram and the genus 1 trisection diagram of S^4 depicted in Figure 1. The reverse operation is called a *destabilisation*.

Note that this (de)stabilisation is the unbalanced one.

Every 4-manifold admits a trisection, and any two trisections of the same 4-manifold are isotopic after performing some number of stabilisations [**5**]. As a corollary, it is known that any two closed 4-manifolds are diffeomorphic if and only if two corresponding trisection diagrams are related by surface diffeomorphisms, handle slides among the same family curves and balanced stabilisations.

https://doi.org/10.1017/S0305004125101746 Published online by Cambridge University Press

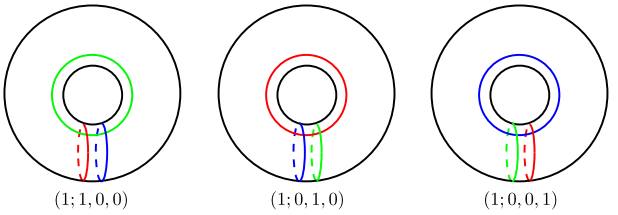


Figure 1. The genus 1 trisection diagrams of S^4.

Let X and Y be diffeomorphic closed 4-manifolds. Two trisections (X_1, X_2, X_3) of X and (Y_1, Y_2, Y_3) of Y are *diffeomorphic* if there exists a diffeomorphism $h\colon X \to Y$ such that $h(X_i) = Y_i$ for each $i = 1, 2, 3$. Two trisections (X_1, X_2, X_3) and (Y_1, Y_2, Y_3) of a 4-manifold Z are *isotopic* if there exists an isotopy $h_t\colon Z \to Z$ such that $h_0 = id_Z$ and $h_1(X_i) = Y_i$ for each $i = 1, 2, 3$. Two trisections are diffeomorphic if and only if two corresponding trisection diagrams are related without stabilisations. It is conjectured that each trisection of S^4 is isotopic to the genus-0 trisection or its stabilisation [**15**]. A counterexample of this conjecture may be given via trisection diagrams of a 4-manifold diffeomorphic to S^4 since any two isotopic trisections are diffeomorphic.

Trisections of 4-manifolds with boundary are called *relative trisections* [**1**]. We recall them here. For the disk $D = \{re^{i\theta} \mid r \in [0, 1], -\pi/3 \leq \theta \leq \pi/3\} \subset \mathbb{C}$, let

$$\partial^- D = \{re^{\pi/3} \in \partial D \mid r \in [0, 1]\},$$

$$\partial^0 D = \{e^{i\theta} \in \partial D\} \text{ and}$$

$$\partial^+ D = \{re^{-\pi/3} \in \partial D \mid r \in [0, 1]\}.$$

Then, $\partial D = \partial^- D \cup \partial^0 D \cup \partial^+ D$. For a genus p surface P with b boundary components, $U := P \times D$ is diffeomorphic to $\natural_{2p+b-1} S^1 \times B^3$. Furthermore, its boundary is decomposed into $\partial^0 U = (P \times \partial^0 D) \cup (\partial P \times D)$ and $\partial^\pm U = P \times \partial^\pm D$. Let V_n be $\natural_n(S^1 \times B^3)$ and $\partial V_n = H_s^- \cup H_s^+$ a genus $n + s$ Heegaard splitting of ∂V_n.

Let $s = g - k + p + b - 1$ and $n = k - 2p - b + 1$. Then, we have $Z_k \cong U \natural V_n \cong \natural_k S^1 \times B^3$. Note that

$$\partial Z_k = Y^+_{g,k;\,p,b} \cup Y^0_{g,k;\,p,b} \cup Y^-_{g,k;\,p,b},$$

where $Y^\pm_{g,k;\,p,b} = \partial^\pm U \natural H_s^\pm$ and $Y^0_{g,k;\,p,b} = \partial^0 U$. Under the above settings, we define relative trisections as follows.

Definition 2·4. Let W be a 4-manifold with connected boundary. A decomposition $W = W_1 \cup W_2 \cup W_3$ of W is called a $(g, k; p, b)$-*relative trisection* of W if the followings hold:

(i) $W_i \cong Z_k$ for $i = 1, 2, 3$;
(ii) $W_i \cap W_{i+1} \cong Y^+_{g,k;\,p,b}$ and $W_i \cap W_{i-1} \cong Y^-_{g,k;\,p,b}$ for $i = 1, 2, 3$.

It follows from these conditions that $W_1 \cap W_2 \cap W_3$ is a genus g surface with b boundary components.

https://doi.org/10.1017/S0305004125101746 Published online by Cambridge University Press

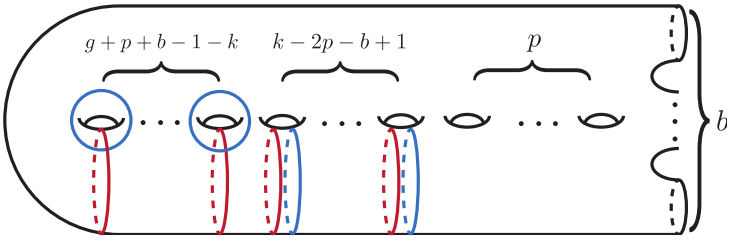


Figure 2. The standard diagram for relative trisection diagrams.

As in the closed case, *relative trisection diagrams* can be defined for relative trisections [**2**].

Definition 2·5. For a genus g surface Σ with b boundary components and three sets of $g-p$ simple closed curves α, β and γ on Σ, a $(g,k;p,b)$- *relative trisection diagram* is a 4-tuple $(\Sigma;\alpha,\beta,\gamma)$ such that each of $(\Sigma;\alpha,\beta)$, $(\Sigma;\beta,\gamma)$ and $(\Sigma;\gamma,\alpha)$ is related to the diagram depicted in Figure 2 by surface diffeomorphisms and handle slides.

Arced relative trisection diagrams, which are needed when we consider gluing two relative trisection diagrams, are defined for relative trisection diagrams.

Definition 2·6. Let $(\Sigma,\alpha,\beta,\gamma)$ be a $(g,k;p,b)$-relative trisection diagram, and $\mathfrak{a}$, $\mathfrak{b}$ and $\mathfrak{c}$ collections of $2p$ properly embedded arcs in Σ. Suppose that the arcs $\mathfrak{a}$ (resp. $\mathfrak{b}$ and $\mathfrak{c}$) are disjoint from α (resp. β and γ). A tuple $(\Sigma,\alpha,\beta,\gamma,\mathfrak{a},\mathfrak{b},\mathfrak{c})$ is called *an arced relative trisection diagram* if the following conditions hold:

(i) cutting Σ_α (resp. Σ_β, Σ_γ) along $\mathfrak{a}$ (resp. $\mathfrak{b}$, $\mathfrak{c}$) yields a disk, where Σ_x is a surface obtained by surgering Σ along x for $x\in\{\alpha,\beta,\gamma\}$;

(ii) by handle slides, $(\Sigma,\alpha,\beta,\mathfrak{a},\mathfrak{b})$ is related to some $(\Sigma,\alpha',\beta',\mathfrak{a}',\mathfrak{b}')$ such that (Σ,α',β') is related to the diagram shown in Figure 2 and $\mathfrak{a}'=\mathfrak{b}'$;

(iii) by handle slides, $(\Sigma,\beta,\gamma,\mathfrak{b},\mathfrak{c})$ is related to some $(\Sigma,\beta',\gamma',\mathfrak{b}',\mathfrak{c}')$ such that (Σ,β',γ') is related to the diagram shown in Figure 2 and $\mathfrak{b}'=\mathfrak{c}'$.

An algorithm for drawing the arcs is developed in [**2**, theorem 5].

THEOREM 2·7 ([**2**, theorem 5]). *Let $(\Sigma,\alpha,\beta,\gamma)$ be a relative trisection diagram and Σ_α the surface obtained by surgering Σ along α and $\phi\colon \Sigma\backslash\alpha\to\Sigma_\alpha$ an associated embedding. Then, collections $\mathfrak{a}$, $\mathfrak{b}$ and $\mathfrak{c}$ of arcs in Σ are obtained by taking the procedure below in order.*

(i) *There exists a collection of properly embedded arcs δ in Σ_α such that cutting Σ_α along δ produces the disk. Then, let $\mathfrak{a}$ denote a collection of properly embedded arcs in $\Sigma-\alpha$ such that δ is isotopic to $\phi(\mathfrak{a})$ in Σ_α.*

(ii) *A collection of arcs in Σ that is disjoint from β can be obtained by sliding a copy of $\mathfrak{a}$ over α. Then, let $\mathfrak{b}$ denote the collection of arcs. Note that in this operation, sliding a β curve over other β curves can be performed if necessary.*

https://doi.org/10.1017/S0305004125101746 Published online by Cambridge University Press

(iii) *A collection of arcs in* Σ *that is disjoint from* γ *can be obtained by sliding a copy of* $\mathfrak{b}$ *over* β. *Then, let* $\mathfrak{c}$ *denote the collection of arcs. Note that in this operation, sliding a* γ *curve over other* γ *curves can be performed if necessary.*

2·2. *Doubly pointed Heegaard/trisection diagrams*

We first recall bridge decompositions of classical knots in 3-manifolds.

Definition 2·8. Let H be a 3-dimensional 1-handlebody and $\tau = \{\tau_i\}$ a collection of arcs properly embedded in H. We say that τ is *trivial* if τ_i can be isotoped into ∂H for each i, or equivalently, there exists a collection $\Delta = \{\Delta_i\}$ of disks in H with $\Delta_i \cap \Delta_j = \emptyset$ such that $\partial \Delta_i = \tau_i \cup \tau_i'$ for some arc $\tau_i' \subset \partial H$. We call τ, Δ and τ_i' *trivial tangles*, *bridge disks* and a *shadow* of τ_i, respectively.

Let $M = H_1 \cup H_2$ be a Heegaard splitting of a closed 3-manifold M and K a knot in M. For a positive integer b, a decomposition $(M, K) = (H_1, H_1 \cap K) \cup (H_2, H_2 \cap K)$ of (M,K) is called a *b-bridge decomposition* if $H_i \cap K$ consists of b trivial arcs for $i = 1, 2$. It is known that every knot admits a 1-bridge decomposition by meridional stabilisations. A knot admitting a 1-bridge decomposition can be described by a *doubly pointed Heegaard diagram* which is a Heegaard diagram $(\Sigma, \alpha, \beta, z, w)$ of the 3-manifold with two base points z and w on Σ that are disjoint from α and β. The union of two arcs connecting the two base points in each handlebody of the Heegaard splitting describes the knot, and a knot can be determined uniquely by the two base points. For more details, see [**19**] for example.

Similar to bridge decompositions of classical knots in 3-manifolds, *bridge trisections* of surface knots in 4-manifolds are introduced in [**16, 17**].

Definition 2·9. Let V be a 4-dimensional 1-handlebody and $\mathcal{D}$ a collection of disks properly embedded in V. We say that $\mathcal{D}$ is *trivial* if the disks of $\mathcal{D}$ can be simultaneously isotoped into ∂V.

Definition 2·10. Let $X = X_1 \cup X_2 \cup X_3$ be a $(g; k_1, k_2, k_3)$-trisection of a closed 4-manifold X, and S a surface-knot in X. A decomposition $(X, S) = (X_1, \mathcal{D}_1) \cup (X_2, \mathcal{D}_2) \cup (X_3, \mathcal{D}_3)$ is called a $(g; k_1, k_2, k_3; b; c_1, c_2, c_3)$-*bridge trisection* of (X,S) if the following hold:

(i) for each $i = 1, 2, 3$, $\mathcal{D}_i$ is a collection of c_i trivial disks in X_i;
(ii) for $i \neq j$, the intersection $\mathcal{D}_i \cap \mathcal{D}_j$ forms b trivial tangles in $X_i \cap X_j$.

We say that S is in $(b; c_1, c_2, c_3)$-*bridge position* with respect to the trisection (X_1, X_2, X_3) if $(X, S) = (X_1, S \cap X_1) \cup (X_2, S \cap X_2) \cup (X_3, S \cap X_3)$ is a $(g; k_1, k_2, k_3; b; c_1, c_2, c_3)$-bridge trisection. In particular, if $c_1 = c_2 = c_3$, we simply say that S is in b-bridge position.

Definition 2·11. Let $(X, S) = (X_1, \mathcal{D}_1) \cup (X_2, \mathcal{D}_2) \cup (X_3, \mathcal{D}_3)$ be a bridge trisection. A 4-tuple $(\Sigma, (\alpha, \mathfrak{a}), (\beta, \mathfrak{b}), (\gamma, \mathfrak{c}))$ is called a *shadow diagram* if the 4-tuple $(\Sigma, \alpha, \beta, \gamma)$ is a trisection diagram of the trisection (X_1, X_2, X_3) of X, and $\mathfrak{a}$, $\mathfrak{b}$ and $\mathfrak{c}$ are shadows of $\mathcal{D}_1 \cap \mathcal{D}_2$, $\mathcal{D}_2 \cap \mathcal{D}_3$ and $\mathcal{D}_3 \cap \mathcal{D}_1$, respectively. In particular, if each of $\mathfrak{a}$, $\mathfrak{b}$ and $\mathfrak{c}$ consists of one shadow of $\mathcal{D}_i \cap \mathcal{D}_j$, the shadow diagram is called a *doubly-pointed trisection diagram*.

https://doi.org/10.1017/S0305004125101746 Published online by Cambridge University Press

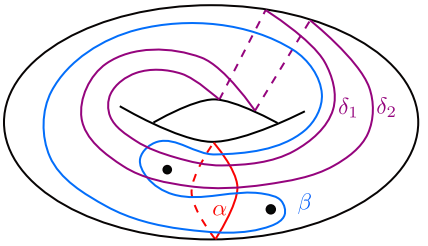


Figure 3. A doubly-pointed Heegaard diagram of $(S^3, T(3,2))$ and the curves δ_1 and δ_2.

Similar to doubly-pointed Heegaard diagrams, for a trisection diagram $(\Sigma, \alpha, \beta, \gamma)$, a doubly-pointed trisection diagram is often denoted by $(\Sigma, \alpha, \beta, \gamma, z, w)$, where z and w are two base points on Σ that are disjoint from α, β and γ. It is known that every 2-knot can be put in 1-bridge position by meridional stabilisations [**16, 17**]. Namely, every 2-knot can be described by a doubly-pointed trisection diagram. The union of three arcs connecting the two base points in each sector of the trisection describes the 2-knot, and a 2-knot can be determined uniquely by the two base points. See [**16, 17**] for more details.

3. *Constructing trisection diagrams for Gluck twisting*

In this section, we construct the trisection diagram (Lemma 3·3) in Question 1·1 for the spun $(p+1, p)$-torus knot $S(T(p+1,p))$, where $T(p+1,p)$ denotes the $(p+1,p)$-torus knot. The construction is similar to the one in [**11**, section 3]. Note that t_c denotes the right-handed Dehn twist along a simple closed curve c.

LEMMA 3·1. *Let $(\Sigma, \alpha, \beta, z, w)$ be a doubly-pointed Heegaard diagram of $(S^3, T(3,2))$ depicted in Figure 3. Then, for $p \geq 2$, $(\Sigma, \alpha, t_{\delta_1}^{p-2} t_{\delta_2}^{-(p-2)}(\beta), z, w)$ is a doubly-pointed Heegaard diagram of $(S^3, T(p+1,p))$, where δ_1 and δ_2 are the curves depicted in Figure 3.*

Proof. Figure 4 is the doubly-pointed Heegaard diagram $(\Sigma, \alpha, t_{\delta_1}^{p-2} t_{\delta_2}^{-(p-2)}(\beta), z, w)$. Note that $(\Sigma, \alpha, t_{\delta_1}^{p-2} t_{\delta_2}^{-(p-2)}(\beta))$ is a Heegaard diagram of S^3 since δ_1 and δ_2 can be parallel in the Heegaard diagram. Then, arcs a and b for α and $t_{\delta_1}^{p-2} t_{\delta_2}^{-(p-2)}(\beta)$, respectively, can be drawn as in Figure 4. The union $a \cup b$ describes the $(p+1,p)$-torus knot $T(p+1,p)$. This completes the proof.

Figure 5 is the doubly-pointed Heegaard diagram $(\Sigma, \alpha, t_{\delta_1} t_{\delta_2}^{-1}(\beta), z, w)$ of $(S^3, T(4,3))$ for example. Lemma 3·1 corresponds to [**11**, lemma 3·6] in the case of $(S^4, T(2n+1,2))$.

LEMMA 3·2. *Let $(\Sigma, \alpha, \beta, \gamma, a, b, c)$ be an arced relative trisection diagram of $S^4 - S(T(3,2))$ depicted in Figure 6. Then, for $p \geq 2$, $(\Sigma, \alpha', \beta', \gamma', a', b', c')$ is an arced relative trisection diagram of $S^4 - S(T(p+1,p))$, where*:

(i) $\alpha' = (t_{\delta_1^\beta}^{p-2} t_{\delta_2^\beta}^{-(p-2)}(\alpha_1), \alpha_2, \alpha_3)$;

(ii) $\beta' = (t_{\delta_1^\beta}^{p-2} t_{\delta_2^\beta}^{-(p-2)}(\beta_1), \beta_2, \beta_3)$;

(iii) $\gamma' = (t_{\delta_1^\gamma}^{p-2} t_{\delta_2^\gamma}^{-(p-2)}(\gamma_1), \gamma_2, \gamma_3)$;

https://doi.org/10.1017/S0305004125101746 Published online by Cambridge University Press

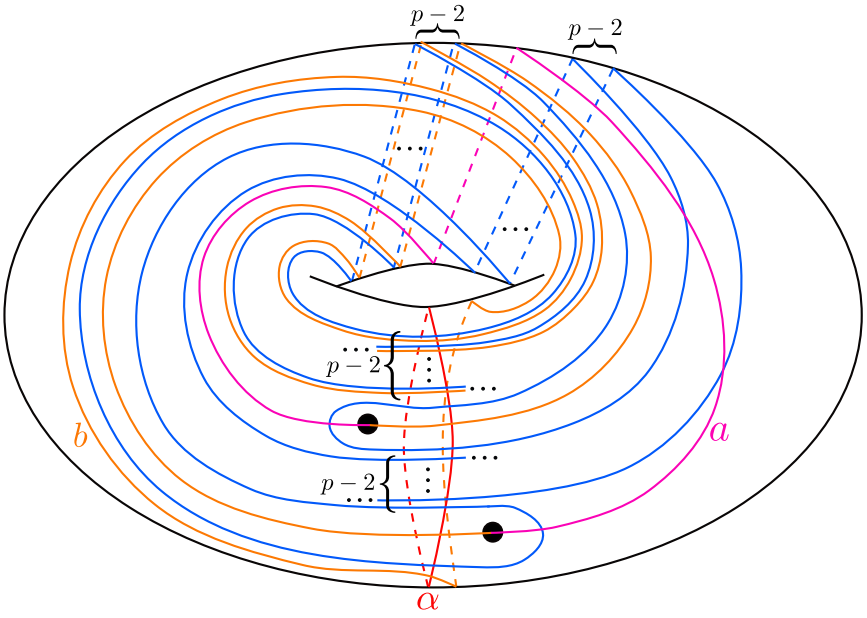


Figure 4. The doubly-pointed Heegaard diagram $(\Sigma, \alpha, t_{\delta_1}^{p-2} t_{\delta_2}^{-(p-2)}(\beta), z, w)$ of $(S^3, T(p+1,p))$ and arcs a and b. The union $a \cup b$ describes $T(p+1,p)$.

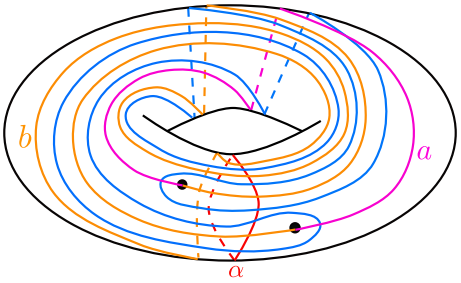


Figure 5. The doubly-pointed Heegaard diagram $(\Sigma, \alpha, t_{\delta_1} t_{\delta_2}^{-1}(\beta), z, w)$ of $(S^3, T(4,3))$ and arcs a and b. The union $a \cup b$ describes $T(4,3)$.

(iv) $a' = t_{\delta_1^\beta}^{p-2} t_{\delta_2^\beta}^{-(p-2)}(a)$;

(v) $b' = t_{\delta_1^\beta}^{p-2} t_{\delta_2^\beta}^{-(p-2)}(b)$;

(vi) $c' = t_{\delta_1^\gamma}^{p-2} t_{\delta_2^\gamma}^{-(p-2)}(c)$;

and the curves δ_1^β, δ_2^β, δ_1^γ and δ_2^γ are the ones depicted in Figure 6.

Proof. By applying Meier's spinning method [**14**] (see also [**11**, subsection 3·1]) to Lemma 3·1 and Figure 3, we have a doubly-pointed trisection diagram of $(S^4, S(T(p+1,p)))$. See [**11**, figure 4 and lemma 3·7] in the case of $(S^4, S(T(2n+1,2)))$. Then, by removing a neighbourhood of the base points (two black points z and w) of the doubly-pointed trisection diagram, we get a relative trisection diagram of $S^4 - S(T(p+1,p))$. See [**11**, figure 5 and

https://doi.org/10.1017/S0305004125101746 Published online by Cambridge University Press

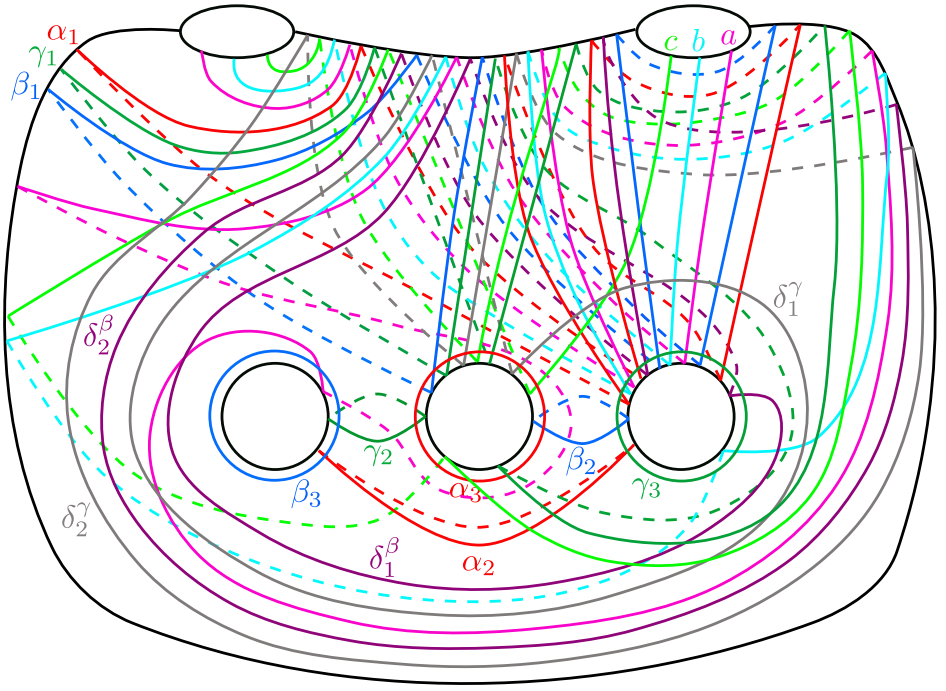


Figure 6. An arced relative trisection diagram of $S^4 - S(T(3,2))$ and the curves δ_1^β, δ_2^β, δ_1^γ and δ_2^γ. See also Figure 7 for visual clarity.

lemma 3·8] in the case of $(S^4, S(T(2n+1,2)))$. Lastly, by using an algorithm for drawing arcs of relative trisection diagrams [**2**] (see also [**11**, subsection 3·3]), we obtain an arced relative trisection diagram of $S^4 - S(T(p+1,p))$. See [**11**, figure 6 and lemma 3·9] in the case of $(S^4, S(T(2n+1,2)))$. This completes the proof.

Figure 7 describes α, β and γ curves and arcs in Figure 6. Lemma 3·2 corresponds to [**11**, lemma 3·9].

LEMMA 3·3. *Let $(\Sigma, \alpha, \beta, \gamma)$ be a trisection diagram obtained by Gluck twisting on the spun trefoil knot depicted in Figure 8, using the methods of* [**6**]. *Then, for $p \geq 2$, $(\Sigma, \alpha', \beta', \gamma')$ is a trisection diagram obtained by Gluck twisting on $S(T(p+1,p))$ using the same methods, where:*

(i) $\alpha' = (t_{\delta_1^\beta}^{p-2} t_{\delta_2^\beta}^{-(p-2)}(\alpha_1), \alpha_2, \alpha_3, t_{\delta_1^\beta}^{p-2} t_{\delta_2^\beta}^{-(p-2)}(\alpha_4), \alpha_5, \alpha_6)$;

(ii) $\beta' = (t_{\delta_1^\beta}^{p-2} t_{\delta_2^\beta}^{-(p-2)}(\beta_1), \beta_2, \beta_3, t_{\delta_1^\beta}^{p-2} t_{\delta_2^\beta}^{-(p-2)}(\beta_4), \beta_5, \beta_6)$;

(iii) $\gamma' = (t_{\delta_1^\gamma}^{p-2} t_{\delta_2^\gamma}^{-(p-2)}(\gamma_1), \gamma_2, \gamma_3, t_{\delta_1^\gamma}^{p-2} t_{\delta_2^\gamma}^{-(p-2)}(\gamma_4), \gamma_5, \gamma_6)$;

and the curves δ_1^β, δ_2^β, δ_1^γ and δ_2^γ are the ones depicted in Figure 8.

Proof. Gay and Meier [**6**] showed that for a closed 4-manifold X and a 2-knot K in X, a trisection diagram of $\Sigma_K(X)$ is obtained by gluing an arced relative trisection diagram of the

https://doi.org/10.1017/S0305004125101746 Published online by Cambridge University Press

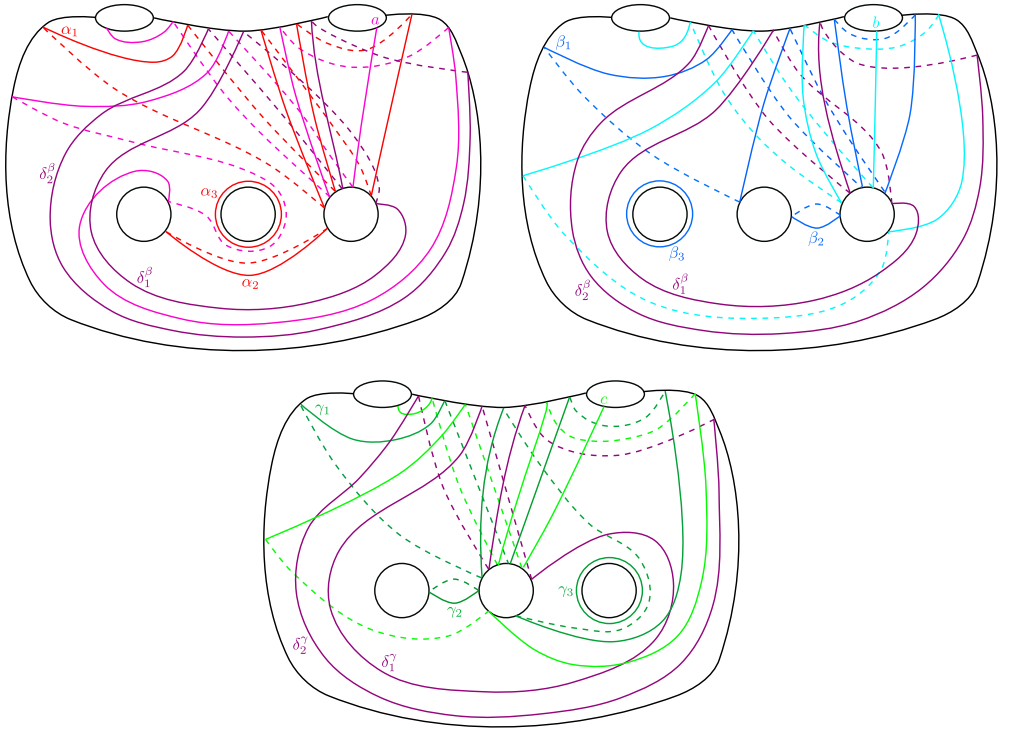


Figure 7. α curves and arc (top left), β curves and arc (top right) and γ curves and arc (bottom) in Figure 6 for visual clarity.

exterior of K and Figure 12 (a). Thus, we can obtain a trisection diagram of $\Sigma_{S(T(p+1,p))}(S^4)$ by gluing Figure 6, or equivalently, Figure 7 and Figure 12 (a), which is depicted in Figure 8. This completes the proof.

Lemma 3·3 corresponds to [**11**, lemma 3·11].
We represent the choice of arcs used for handle slides by using the notation in Figure 9.

LEMMA 3·4. *Let a, b and c be simple closed curves in a surface. Suppose that a does not intersect with both of b and c, and that b intersects with c m times. Let d be a simple closed curve obtained by handle sliding c over a ℓ times along arcs $a_1, \dots, a_\ell$. Then, for any integer n, the simple closed curve $t_d^n(b)$ is isotopic to the simple closed curve obtained by handle sliding $t_c^n(b)$ over a $\ell \cdot m \cdot |n|$ times along the arcs $a_1, \dots, a_\ell$.*

Proof. A schematic diagram depicted in Figure 10 completes the proof in the case where $\ell = m = 1$ and n is positive. The other cases can be shown in a similar way.

Remark 3·5. Due to this lemma, we can deform trisection diagrams by handle sliding the twisting curve c over curves of the trisection diagrams while preserving the diffeomorphism types of trisections and 4-manifolds corresponding to the trisection diagrams (see Figure 11 for example). We use this lemma repeatedly in this paper to simplify deformations of trisection diagrams.

https://doi.org/10.1017/S0305004125101746 Published online by Cambridge University Press

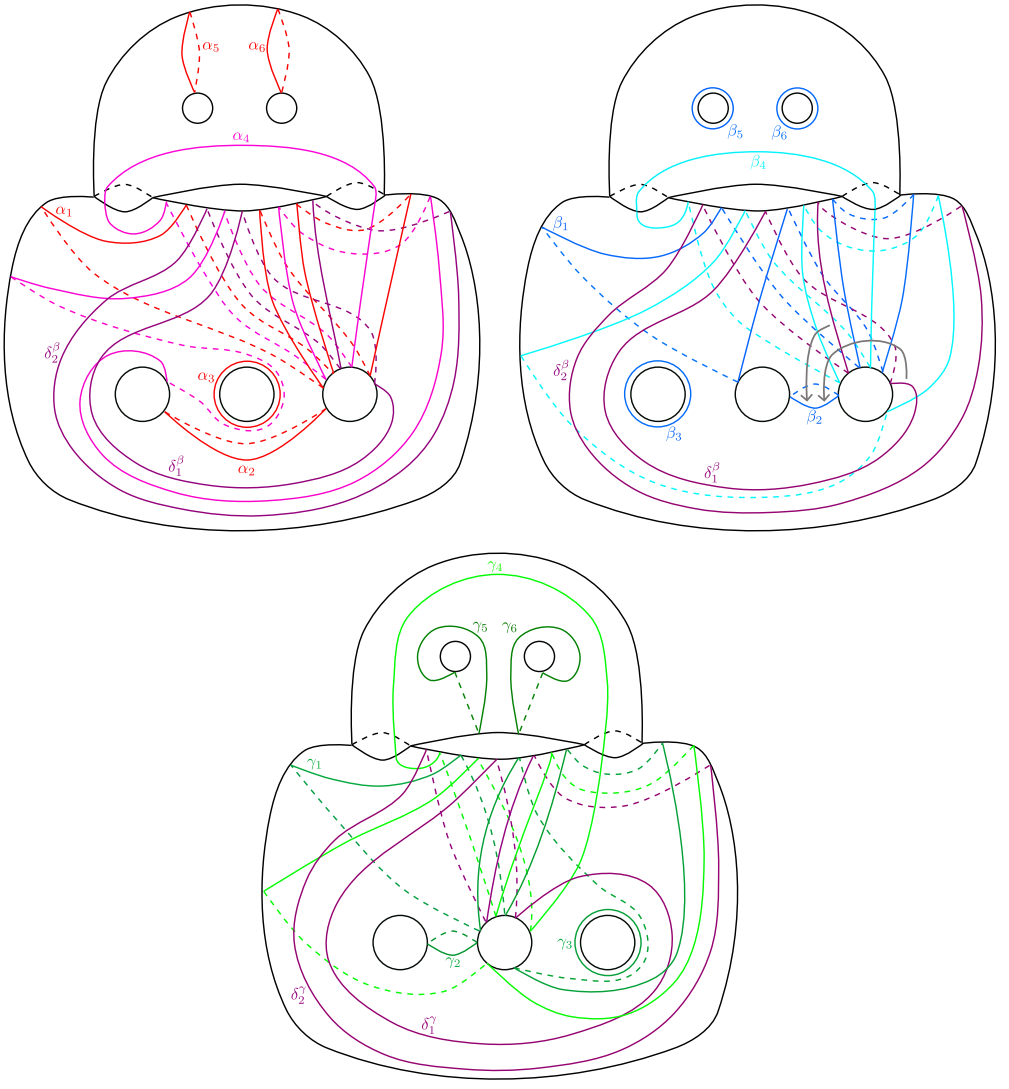


Figure 8. A trisection diagram obtained by Gluck twisting on the spun trefoil and the curves δ_1^β, δ_2^β, δ_1^γ and δ_2^γ. The trisection diagram of $\Sigma_{S(T(p+1,p))}(S^4)$ is $(\Sigma, \alpha', \beta', \gamma')$, where $\alpha' = (t_{\delta_1^\beta}^{p-2} t_{\delta_2^\beta}^{-(p-2)}(\alpha_1), \alpha_2, \alpha_3, t_{\delta_1^\beta}^{p-2} t_{\delta_2^\beta}^{-(p-2)}(\alpha_4), \alpha_5, \alpha_6)$, $\beta' = (t_{\delta_1^\beta}^{p-2} t_{\delta_2^\beta}^{-(p-2)}(\beta_1), \beta_2, \beta_3, t_{\delta_1^\beta}^{p-2} t_{\delta_2^\beta}^{-(p-2)}(\beta_4), \beta_5, \beta_6)$ and $\gamma' = (t_{\delta_1^\gamma}^{p-2} t_{\delta_2^\gamma}^{-(p-2)}(\gamma_1), \gamma_2, \gamma_3, t_{\delta_1^\gamma}^{p-2} t_{\delta_2^\gamma}^{-(p-2)}(\gamma_4), \gamma_5, \gamma_6)$ (Lemma 3·3).

LEMMA 3·6. *The trisection diagram of $\Sigma_{S(T(p+1,p))}(S^4)$ shown in Figure 14 can be obtained by destabilising the trisection diagram of $\Sigma_{S(T(p+1,p))}(S^4)$ shown in Figure 8 twice.*

Proof. In Figure 8, firstly perform $t_{\beta_5}^{-1}$ for the entire diagram. Then, handle slide β_5 and the resulting α_5 over β_4 and α_4, respectively, as indicated in Figure 12 (*a*) to resolve the intersections of the resulting γ_5 and both β_5 and the resulting α_5. Then, since α_4 and β_4 can be parallel by handle slides due to Theorem 2·7, we can destabilise the trisection diagram shown in Figure 8 for α_4 (precisely $t_{\delta_1^\beta}^{p-2} t_{\delta_2^\beta}^{-(p-2)}(\alpha_4)$), β_4 (precisely $t_{\delta_1^\beta}^{p-2} t_{\delta_2^\beta}^{-(p-2)}(\beta_4)$) and the

https://doi.org/10.1017/S0305004125101746 Published online by Cambridge University Press

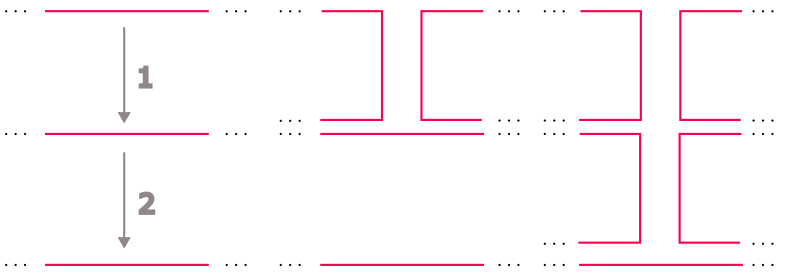


Figure 9. Arcs used for handle slides are indicated by arrows as in this figure. The left-hand figure means that firstly we perform the handle slide labelled 1 (the central figure), and then we perform the handle slide labelled 2 (the right-hand figure).

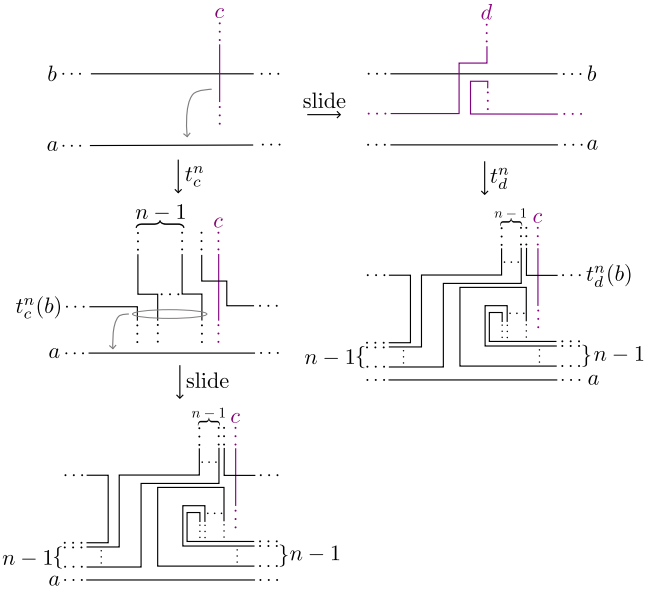


Figure 10. A schematic diagram of Lemma 3·4 in the case where $\ell = m = 1$ and n is positive.

resulting γ_5. By the destabilisation, we have the trisection diagram $\mathcal{D}_1$ obtained by gluing Figure 7 and Figure 12 (b). See also [**6**, figure 15]. Note that this destabilisation is based on Naylor's method (Lemma 8 in [**18**]).

In the trisection diagram $\mathcal{D}_1$, slide β_6 and γ_6 over β_5 and γ_4, respectively, as indicated in Figure 12 (b). Then, since γ_4 and the resulting β_6 can be parallel by handle slides due to Theorem 2·7 and δ_i^β can be parallel to δ_i^γ by sliding δ_i^β over β_2 in Figure 7 or 8 as indicated in Figure 8 for $i = 1, 2$, we can destabilise $\mathcal{D}_1$ for α_6, the resulting β_6 (precisely $t_{\delta_1^\beta}^{p-2} t_{\delta_2^\beta}^{-(p-2)}(\beta_6)$) and γ_4 (precisely $t_{\delta_1^\gamma}^{p-2} t_{\delta_2^\gamma}^{-(p-2)}(\gamma_4)$) due to Lemma 3·4. By the destabilisation, we have the trisection diagram $\mathcal{D}_2$ obtained by gluing Figure 7 and Figure 13 (c). Note that this destabilisation is also based on Naylor's method [**18**, lemma 8].

In the trisection diagram $\mathcal{D}_2$, by performing t_c^{-1} for Figure 13 (a), we have the trisection diagram obtained by gluing Figure 7 and Figure 13 (b), which is just the trisection diagram shown in Figure 14.

https://doi.org/10.1017/S0305004125101746 Published online by Cambridge University Press

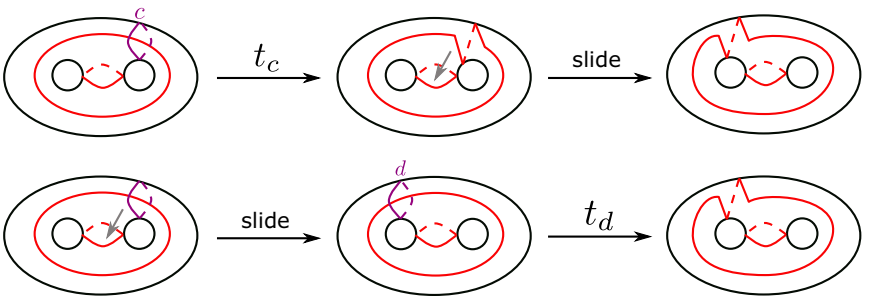


Figure 11. This figure describes a simple example of Lemma 3·4 for α curves of a trisection diagram. In the upper column, we perform firstly the Dehn twist, and then handle sliding as indicated in the figure. This is a usual deformation for trisection diagrams. In the lower column, we firstly handle slide c over the α curve in the same way as the upper column, and then perform the Dehn twist. The resulting two α curves are the same.

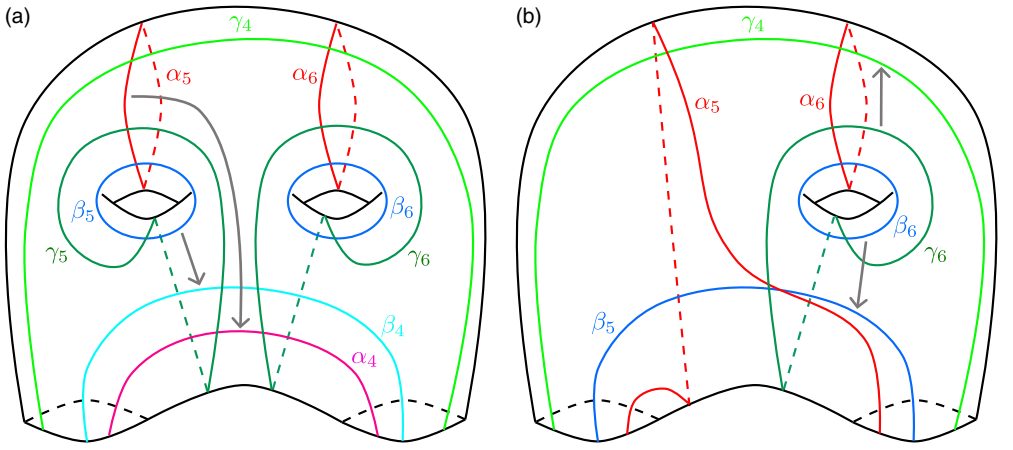


Figure 12. (Left) A part of the trisection diagram shown in Figure 8. (Right) A part of the trisection diagram $\mathcal{D}_1$ obtained by destabilising the trisection diagram shown in Figure 8 once.

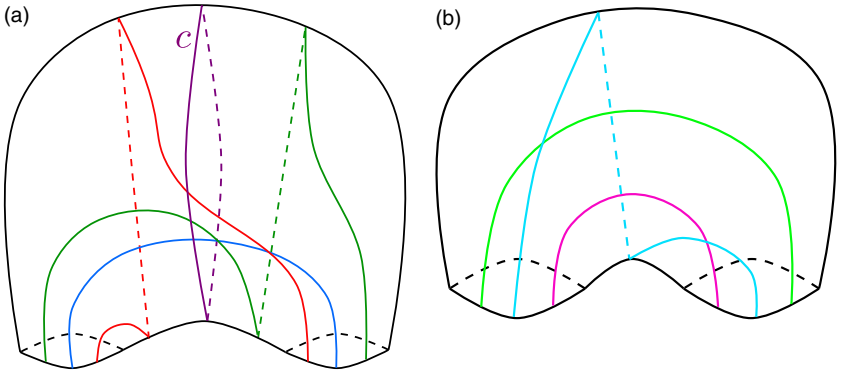


Figure 13. (Left) A part of the trisection diagram $\mathcal{D}_2$ obtained by destabilising the trisection diagram $\mathcal{D}_1$ once. (Right) A part of the trisection diagram obtained by performing t_c^{-1} for $\mathcal{D}_2$.

https://doi.org/10.1017/S0305004125101746 Published online by Cambridge University Press

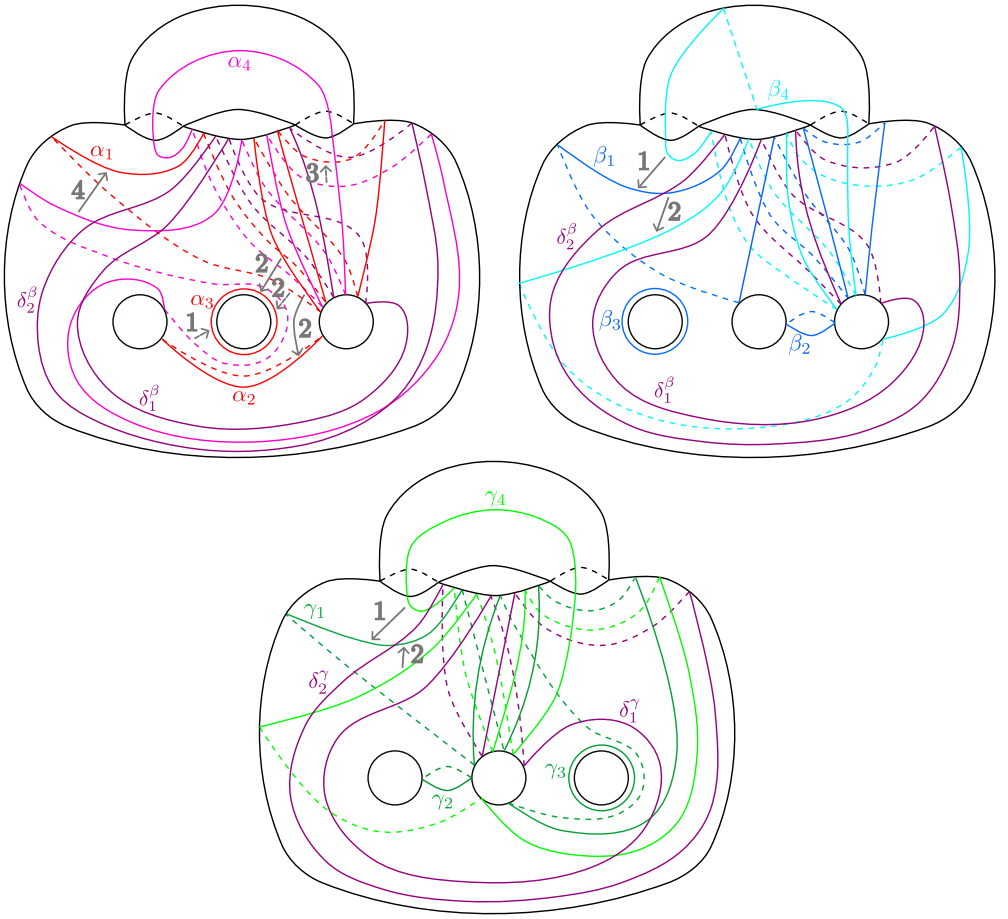


Figure 14. A trisection diagram obtained by Gluck twisting on the spun trefoil and the curves δ_1^β, δ_2^β, δ_1^γ and δ_2^γ. The trisection diagram of $\Sigma_{S(T(p+1,p))}(S^4)$ is $(\Sigma, \alpha', \beta', \gamma')$, where $\alpha' = (t_{\delta_1^\beta}^{p-2} t_{\delta_2^\beta}^{-(p-2)}(\alpha_1), \alpha_2, \alpha_3, t_{\delta_1^\beta}^{p-2} t_{\delta_2^\beta}^{-(p-2)}(\alpha_4))$, $\beta' = (t_{\delta_1^\beta}^{p-2} t_{\delta_2^\beta}^{-(p-2)}(\beta_1), \beta_2, \beta_3, t_{\delta_1^\beta}^{p-2} t_{\delta_2^\beta}^{-(p-2)}(\beta_4))$ and $\gamma' = (t_{\delta_1^\gamma}^{p-2} t_{\delta_2^\gamma}^{-(p-2)}(\gamma_1), \gamma_2, \gamma_3, t_{\delta_1^\gamma}^{p-2} t_{\delta_2^\gamma}^{-(p-2)}(\gamma_4))$.

None of the operations above change the diffeomorphism type of the 4-manifold. Thus, the trisection diagram shown in Figure 14 describes the Gluck twisted 4-manifold $\Sigma_{S(T(p+1,p))}(S^4)$. This completes the proof.

In this paper, we will show in Section 4 that the trisection diagram of $\Sigma_{S(T(p+1,p))}(S^4)$ in Lemma 3·3 is standard for all $p \geq 2$. Namely, we will prove that the trisection diagram can be related to the genus-0 trisection diagram by surface diffeomorphisms, handle slides and destabilisations. Thus, by Lemma 3·6, it suffices to show that the trisection diagram of $\Sigma_{S(T(p+1,p))}(S^4)$ depicted in Figure 14 is standard for all $p \geq 2$.

In Figure 14, we perform the following handle slides in order: slide α_4 over α_3, α_1 over α_2 and α_3, α_4 over α_1 twice, β_4 over β_1, β_1 over β_4, and γ_4 over γ_1 twice. These handle slides are indicated in Figure 14. Then, Figure 15 is obtained. Let $\mathcal{D}_p$ denote this trisection diagram of $\Sigma_{S(T(p+1,p))}(S^4)$, which is obtained by overlaying all of Figure 15.

https://doi.org/10.1017/S0305004125101746 Published online by Cambridge University Press

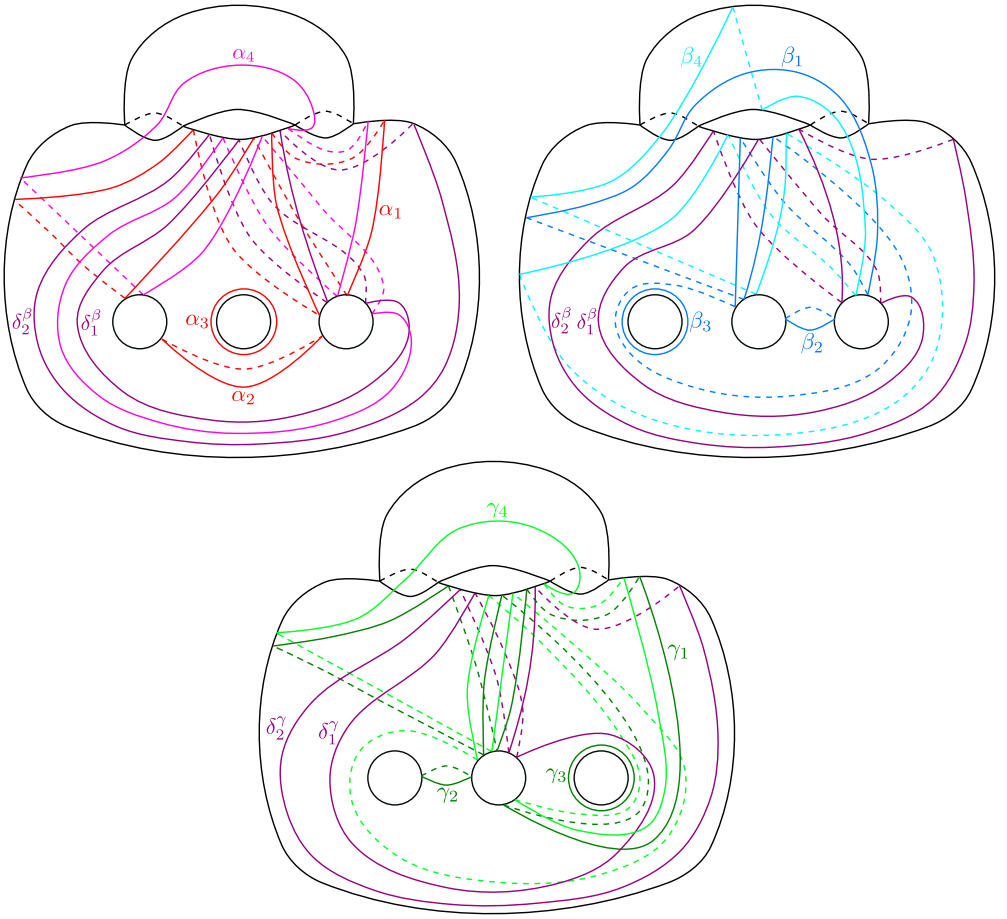


Figure 15. The trisection diagram $\mathcal{D}_p$ of $\Sigma_{S(T(p+1,p))}(S^4)$, where $\alpha = (t_{\delta_1^\beta}^{p-2} t_{\delta_2^\beta}^{-(p-2)}(\alpha_1), \alpha_2, \alpha_3, t_{\delta_1^\beta}^{p-2} t_{\delta_2^\beta}^{-(p-2)}(\alpha_4))$, $\beta = (t_{\delta_1^\beta}^{p-2} t_{\delta_2^\beta}^{-(p-2)}(\beta_1), \beta_2, \beta_3, t_{\delta_1^\beta}^{p-2} t_{\delta_2^\beta}^{-(p-2)}(\beta_4))$ and $\gamma = (t_{\delta_1^\gamma}^{p-2} t_{\delta_2^\gamma}^{-(p-2)}(\gamma_1), \gamma_2, \gamma_3, t_{\delta_1^\gamma}^{p-2} t_{\delta_2^\gamma}^{-(p-2)}(\gamma_4))$.

4. *Main theorem*

In this section, we show the following main theorem mentioned in Section 1.

THEOREM 4·1. *The trisection diagram $\mathcal{D}_p$ ($p \geq 2$) is standard.*

Proof of Theorem 4·1. The proof is mainly divided into two steps. The first step is that we show the trisection diagram $\mathcal{D}_p$ can be destabilised once and destabilise $\mathcal{D}_p$ explicitly. The second step is that we reduce the destabilised trisection diagram to the stabilisation of the genus-0 trisection diagram by an inductive argument. As the inductive argument, we use a key lemma which we call the seesaw lemma. Note that we do not change names of simple closed curves before and after Dehn twists and handle slides unless otherwise stated.

Step 1. Destabilise $\mathcal{D}_p$ once.

https://doi.org/10.1017/S0305004125101746 Published online by Cambridge University Press

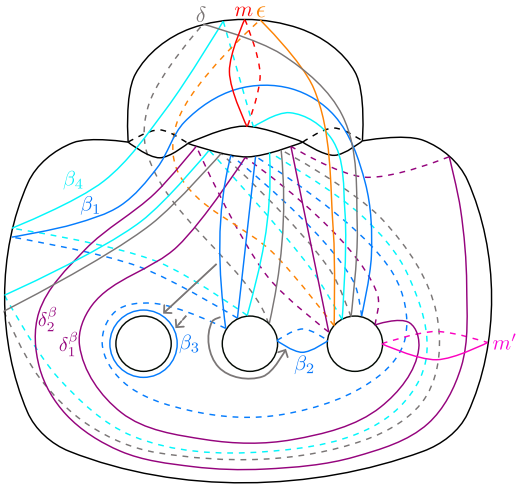


Figure 16. The β curves of $\mathcal{D}_p$ (Figure 15) and curves δ, ϵ, m and m'.

First, we perform Dehn twists $t_\epsilon^{p-2}t_\delta^{-1}$ for $\mathcal{D}_p$, where ϵ and δ are curves in Figure 16. At the beginning, we consider β curves obtained by performing $t_\epsilon^{p-2}t_\delta^{-1}$ for the β curves of $\mathcal{D}_p$. Recall that for a collection of mutually disjoint simple closed curves $C=\{c_1,\dots,c_n\}$ on a surface Σ, Σ_C denotes the surface obtained by surgering Σ along C (see theorem 2·7). We say that two simple closed curves a and b on Σ are *equal ($a=b$) up to handle slide over C (or $c_1,\dots,c_{n-1}$ and c_n)* if they are isotopic on Σ_C.

LEMMA 4·2. *Let $(\Sigma;\beta_1^p,\beta_2,\beta_3,\beta_4^p)$ be the β-curves of $\mathcal{D}_p$, where $\beta_1^p=t_{\delta_1^\beta}^{p-2}t_{\delta_2^\beta}^{-(p-2)}(\beta_1)$ and $\beta_4^p=t_{\delta_1^\beta}^{p-2}t_{\delta_2^\beta}^{-(p-2)}(\beta_4)$ (see Figure 15). Then, the following holds*:

(i) $t_\epsilon^{p-2}t_\delta^{-1}(\beta_2)=\beta_2$ *and* $t_\epsilon^{p-2}t_\delta^{-1}(\beta_3)=\beta_3$;

(ii) $t_\epsilon^{p-2}t_\delta^{-1}(\beta_4^p)=m$ *up to handle slide over* β_2;

(iii) $t_\epsilon^{p-2}t_\delta^{-1}(\beta_1^p)=t_{\delta_1^\beta}^{p-2}(m')$ *up to handle slide over* β_2 *and* β_3;

where δ, ϵ, m and m' are the curves depicted in Figure 16.

Proof. We can immediately check from Figure 16 that $t_\epsilon^{p-2}t_\delta^{-1}(\beta_2)=\beta_2$ and $t_\epsilon^{p-2}t_\delta^{-1}(\beta_3)=\beta_3$ since δ and ϵ do not intersect with β_2 and β_3.

First of all, we show the statement for β_4^p. Since $m=t_\delta^{-1}(\beta_4)$ and curves ϵ, δ, δ_1^β and δ_2^β are all disjoint from β_2 (see Figure 16), it suffices to show that $t_\epsilon^{p-2}t_\delta^{-1}t_{\delta_1^\beta}^{p-2}t_{\delta_2^\beta}^{-(p-2)}(\beta_4)=t_\delta^{-1}(\beta_4)$ up to handle slide over β_2. Since the geometric intersection number of δ_1^β and the other curves is 0, $t_\epsilon^{p-2}t_\delta^{-1}t_{\delta_1^\beta}^{p-2}t_{\delta_2^\beta}^{-(p-2)}(\beta_4)=t_{\delta_1^\beta}^{p-2}t_\epsilon^{p-2}t_\delta^{-1}t_{\delta_2^\beta}^{-(p-2)}(\beta_4)$. Moreover, we can check from Figure 16 that $t_\delta(\epsilon)=\delta_2^\beta$ up to handle slide over β_2. It is well known that $t_{f(c)}=ft_cf^{-1}$ for a simple closed curve c on a surface S and a self-diffeomorphism $f:S\to S$, and that if the geometric intersection number $i(a,b)$ of two simple closed curves a and b is 0, then $t_at_b=t_bt_a$

https://doi.org/10.1017/S0305004125101746 Published online by Cambridge University Press

(for example, see [**3**, fact 3·7 and 3·9], respectively). Thus, the following equalities hold up to handle slide over β_2 (Lemma 3·4):

$$\begin{aligned} t_{\delta_1^\beta}^{p-2} t_\epsilon^{p-2} t_\delta^{-1} t_{\delta_2^\beta}^{-(p-2)}(\beta_4) &= t_{\delta_1^\beta}^{p-2} t_\delta^{-1} t_\delta t_\epsilon^{p-2} t_\delta^{-1} t_{\delta_2^\beta}^{-(p-2)}(\beta_4) \\ &= t_{\delta_1^\beta}^{p-2} t_\delta^{-1} t_{t_\delta(\epsilon)}^{p-2} t_{\delta_2^\beta}^{-(p-2)}(\beta_4) \\ &= t_{\delta_1^\beta}^{p-2} t_\delta^{-1} t_{\delta_2^\beta}^{p-2} t_{\delta_2^\beta}^{-(p-2)}(\beta_4) \\ &= t_\delta^{-1} t_{\delta_1^\beta}^{p-2}(\beta_4). \end{aligned}$$

Thus, it suffices to show $t_\delta^{-1} t_{\delta_1^\beta}^{p-2}(\beta_4) = t_\delta^{-1}(\beta_4)$. This holds obviously since $i(\delta_1^\beta, \beta_4) = 0$ (see Figure 16). Next, we show the statement for β_1^p. We have the following equalities up to handle slide over β_2 (Lemma 3·4):

$$\begin{aligned} t_{\delta_1^\beta}^{-(p-2)} t_\epsilon^{p-2} t_\delta^{-1}(\beta_1^p) &= t_{\delta_1^\beta}^{-(p-2)} t_\epsilon^{p-2} t_\delta^{-1} t_{\delta_1^\beta}^{p-2} t_{\delta_2^\beta}^{-(p-2)}(\beta_1) \\ &= t_\delta^{-1} t_\delta t_\epsilon^{p-2} t_\delta^{-1} t_{\delta_2^\beta}^{-(p-2)}(\beta_1) \\ &= t_\delta^{-1} t_{t_\delta(\epsilon)}^{p-2} t_{\delta_2^\beta}^{-(p-2)}(\beta_1) \\ &= t_\delta^{-1} t_{\delta_2^\beta}^{p-2} t_{\delta_2^\beta}^{-(p-2)}(\beta_1) \\ &= t_\delta^{-1}(\beta_1). \end{aligned}$$

We see from Figure 16 that $t_\delta^{-1}(\beta_1)$ can be parallel to m' after handle sliding over both β_2 and β_3 as indicated in Figure 16. This completes the proof.

Next, we consider α curves obtained by performing $t_\epsilon^{p-2} t_\delta^{-1}$ for the α curves of $\mathcal{D}_p$ (Figure 15 or 19). Recall that the α curves of $\mathcal{D}_p$ are $(t_{\delta_1^\beta}^{p-2} t_{\delta_2^\beta}^{-(p-2)}(\alpha_1), \alpha_2, \alpha_3, t_{\delta_1^\beta}^{p-2} t_{\delta_2^\beta}^{-(p-2)}(\alpha_4))$. Before deforming the α curves, we define the following operation including the Dehn twists, which we call $*_\alpha$: first, perform t_δ^{-1}. Then, slide the resulting α_1 (i.e. $t_\delta^{-1} t_{\delta_1^\beta}^{p-2} t_{\delta_2^\beta}^{-(p-2)}(\alpha_1)$) over the resulting α_3 (i.e. $t_\delta^{-1}(\alpha_3)$, which is the α_3 depicted in the left-hand side of Figure 17) only once as indicated in the left-hand side of Figure 17 to resolve the intersection of the resulting α_1 and ϵ. After that, perform t_ϵ^{p-2}. Finally, slide the resulting α_1 (the α_1 depicted in the right-hand side of Figure 17) and the resulting α_3 (i.e. $t_\epsilon^{p-2} t_\delta^{-1}(\alpha_3)$, which is the α_3 depicted in the right-hand side of Figure 17) over the resulting α_4 (i.e. $t_\epsilon^{p-2} t_\delta^{-1} t_{\delta_1^\beta}^{p-2} t_{\delta_2^\beta}^{-(p-2)}(\alpha_4)$, which is the α_4 depicted in the right-hand side of Figure 17) $p-1$ times each as indicated in the right-hand side of Figure 17 to resolve the intersections of m and both the resulting α_1 and the resulting α_3.

LEMMA 4·3. *The α curves $(t_{\delta_1^\beta}^{p-2} t_{\hat{\delta}}^{-(p-2)}(\alpha_1), \alpha_2, t_{\delta_1^\beta}^{p-2} t_{\tilde{\delta}}^{p-2}(\alpha_3), t_{\delta_1^\beta}^{p-2}(\alpha_4))$ can be obtained by performing the operation $*_\alpha$ for the α curves of $\mathcal{D}_p$ in Figure 15, where α_1, α_3, $\hat{\delta}$ and $\tilde{\delta}$ are the curves depicted in Figure 18.*

https://doi.org/10.1017/S0305004125101746 Published online by Cambridge University Press

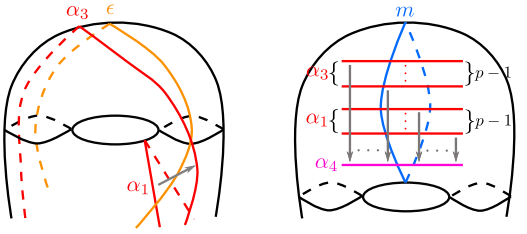


Figure 17. These figures describe how to perform the handle slides in the operation $*_\alpha$. In the left-hand figure, α_1 and α_3 precisely represent $t_\delta^{-1} t_{\delta_1^\beta}^{p-2} t_{\delta_2^\beta}^{-(p-2)}(\alpha_1)$ and $t_\delta^{-1}(\alpha_3)$, respectively, for the α curves of $\mathcal{D}_p$ (i.e. α_1 and α_3 in Figure 15 or 19). In the right-hand figure, α_3 and α_4 precisely represent $t_\epsilon^{p-2} t_\delta^{-1}(\alpha_3)$ and $t_\epsilon^{p-2} t_\delta^{-1} t_{\delta_1^\beta}^{p-2} t_{\delta_2^\beta}^{-(p-2)}(\alpha_4)$, respectively, for the α curves of $\mathcal{D}_p$ (i.e. α_3 and α_4 in Figure 15 or 19). The α_1 in the right-hand figure precisely represents the curve obtained by performing t_ϵ^{p-2} for the curve c obtained by sliding the α_1 in the left-hand figure over the α_3 in the left-hand figure as indicated in the left-hand figure. In fact, $t_\epsilon^{p-2}(c) = c$ since ϵ does not intersect with c due to the slide in the left-hand figure.

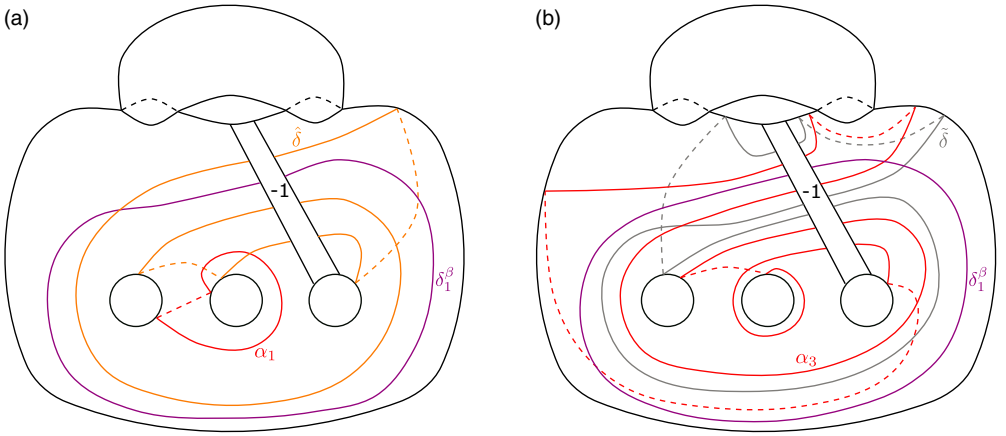


Figure 18. Parts of the α curves obtained by the operation $*_\alpha$ for the α curves in Figure 15. See Figure 20 on the (-1)-box notation.

Proof. It is obvious that $t_{\delta_1^\beta}^{p-2}(\alpha_4)$ is obtained by $*_\alpha$ since both δ and ϵ do not intersect with α_4 and δ_1^β (see Figure 19).

We show firstly the statement for α_1. Since δ_1^β does not intersect with δ_2^β, δ and ϵ (see Figure 19), the operations in $*_\alpha$ which deform α_1 in Figure 15 can be considered as follows: First, perform $t_{\delta_2^\beta}^{-(p-2)}$ and t_δ^{-1} in order. Then, slide the resulting α_1 over $t_\delta^{-1}(\alpha_3)$ as indicated in the left-hand side of Figure 17. After that, slide the resulting α_1 over α_4 $p-1$ times as indicated in the right-hand side of Figure 17. Finally, perform $t_{\delta_1^\beta}^{p-2}$.

Since $t_\delta^{-1} t_{\delta_2^\beta}^{-(p-2)} = t_{t_\delta^{-1}(\delta_2^\beta)}^{-(p-2)} t_\delta^{-1}$, we can take the following operations for α_1 instead of the above operations: first, perform t_δ^{-1} and $t_{t_\delta^{-1}(\delta_2^\beta)}^{-(p-2)}$ in order. Then, slide the resulting α_1 over

https://doi.org/10.1017/S0305004125101746 Published online by Cambridge University Press

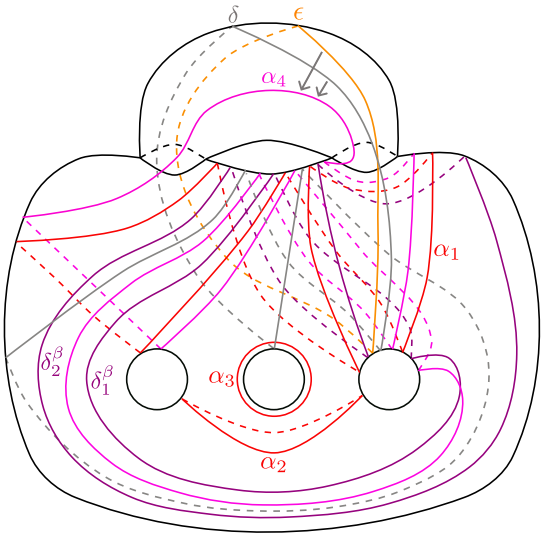


Figure 19. The α curves of $\mathcal{D}_p$ (Figure 15) and curves δ and ϵ.

the resulting α_3 (i.e. $t_\delta^{-1}(\alpha_3)$) as indicated in the left-hand side of Figure 17. After that, slide the resulting α_1 over α_4 $p-1$ times as indicated in the right-hand side of Figure 17. Finally, perform $t_{\delta_1^\beta}^{p-2}$.

The first operation t_δ^{-1} does not deform α_1 in Figure 15 since δ does not intersect with α_1 (see Figure 19). Thus, we can take the following operations: first, perform $t_{t_\delta^{-1}(\delta_2^\beta)}^{-(p-2)}$. Then, slide the resulting α_1 over $t_\delta^{-1}(\alpha_3)$ as indicated in the left-hand side of Figure 17. After that, slide the resulting α_1 over α_4 $p-1$ times as indicated in the right-hand side of Figure 17. Finally, perform $t_{\delta_1^\beta}^{p-2}$.

In these operations, since $t_\delta^{-1}(\delta_2^\beta)$ does not intersect with $t_\delta^{-1}(\alpha_3)$ and α_4 in Figure 15 or 19, we can change the order in the operations as follows: first, slide the α_1 over $t_\delta^{-1}(\alpha_3)$ and α_4 once each as indicated in the left-hand side of Figure 17 and right-hand side of Figure 17, respectively. Then, perform $t_{t_\delta^{-1}(\delta_2^\beta)}^{-(p-2)}$. After that, slide the resulting α_1 over α_4 $p-2$ times as indicated in the right-hand side of Figure 17. Finally, perform $t_{\delta_1^\beta}^{p-2}$.

The first operation, namely, handle sliding α_1 over $t_\delta^{-1}(\alpha_3)$ and α_4, provides us with α_1 in Figure 18 (*a*) up to handle slide over α_2. Thus, the remaining operations for α_1 in Figure 18 (*a*) are as follows: first, perform $t_{t_\delta^{-1}(\delta_2^\beta)}^{-(p-2)}$. After that, slide the resulting α_1 over α_4 $p-2$ times as indicated in the right-hand side of Figure 17. Finally, perform $t_{\delta_1^\beta}^{p-2}$.

Since the simple closed curve $t_\delta^{-1}(\delta_2^\beta)$ does not intersect with α_4 and $t_\delta^{-1}(\delta_2^\beta)$ intersects with α_1 in Figure 18 (*a*) once, the first two operations can be regarded as an operation that performs $t_c^{-(p-2)}$ due to Lemma 3·4, where c is the simple closed curve obtained by sliding $t_\delta^{-1}(\delta_2^\beta)$ over α_4 as indicated in the right-hand side of Figure 17. Actually, c is $\hat{\delta}$. Recall that $\hat{\delta}$ is the curve depicted in Figure 18 (*a*). This completes the proof for α_1.

https://doi.org/10.1017/S0305004125101746 Published online by Cambridge University Press

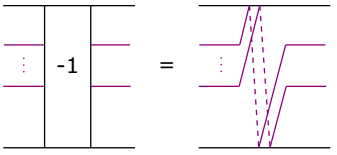


Figure 20. A simple notation for trisection diagrams based on the twist-box notations in Kirby diagrams. This notation simplifies the left-handed Dehn twist.

Next, we show the statement for α_3. In the operation $*_\alpha$, the operations which deform α_3 in Figure 15 are as follows: first, perform t_δ^{-1} and t_ϵ^{p-2} in order. After that, slide the resulting α_3 over α_4 $p-1$ times as indicated in the right-hand side of Figure 17. Finally, perform $t_{\delta_1^\beta}^{p-2}$.

Since δ and ϵ does not intersect with α_4, we can regard these operations as the following operations due to Lemma 3·4: perform $t_{c_1}^{-1}$, $t_{c_2}^{p-2}$ and $t_{\delta_1^\beta}^{p-2}$ in order, where c_1 is the simple closed curve obtained by handle sliding δ over α_4 once as indicated in the right-hand side of Figure 17 (in Figure 19 explicitly) and c_2 is the simple closed curve obtained by handle sliding ϵ over α_4 once as indicated in the right-hand side of Figure 17 (in Figure 19 explicitly). It is obvious that $t_{c_1}^{-1}(\alpha_3)$ for α_3 in Figure 15 is α_3 in Figure 18 (b) and c_2 is $\tilde{\delta}$. Recall that $\tilde{\delta}$ is the curve depicted in Figure 18 (b). This completes the proof for α_3.

Lastly, we consider γ curves obtained by performing $t_\epsilon^{p-2}t_\delta^{-1}$ for the γ curves of $\mathcal{D}_p$ (Figure 15 or 22). Recall that the γ curves of $\mathcal{D}_p$ are $(t_{\delta_1^\gamma}^{p-2}t_{\delta_2^\gamma}^{-(p-2)}(\gamma_1), \gamma_2, \gamma_3, t_{\delta_1^\gamma}^{p-2}t_{\delta_2^\gamma}^{-(p-2)}(\gamma_4))$ for δ_1^γ and δ_2^γ in Figure 15 or 22. Before deforming the γ curves, we define the following operation including the Dehn twists, which we call $*_\gamma$: first, slide δ_1^γ in Figure 15 or 22 over γ_3 of $\mathcal{D}_p$ (Figure 22) as indicated in Figure 22. By this handle slide, δ_1^γ in Figure 21 is obtained. Thus, the γ curves of $\mathcal{D}_p$ can be regarded as $(t_{\delta_1^\gamma}^{p-2}t_{\delta_2^\gamma}^{-(p-2)}(\gamma_1), \gamma_2, \gamma_3, t_{\delta_1^\gamma}^{p-2}t_{\delta_2^\gamma}^{-(p-2)}(\gamma_4))$ for δ_1^γ in Figure 21 and δ_2^γ in Figure 15 or 22 due to Lemma 3·4. Then, perform t_δ^{-1} and t_ϵ^{p-2} in order for the resulting γ curves. After that, slide the resulting γ_3 (i.e. $t_\epsilon^{p-2}t_\delta^{-1}(\gamma_3)$ in Figure 22) over the resulting $t_{\delta_1^\gamma}^{p-2}t_{\delta_2^\gamma}^{-(p-2)}(\gamma_4)$ (i.e. $t_\epsilon^{p-2}t_\delta^{-1}t_{\delta_1^\gamma}^{p-2}t_{\delta_2^\gamma}^{-(p-2)}(\gamma_4)$ in Figure 22, where only δ_1^γ is the curve in Figure 21) only once to resolve the intersection with m in Figure 16. The way of performing the handle slide is similar to the last slide in the operation $*_\alpha$ (see the right-hand side of Figure 17). Note that the resulting $t_{\delta_1^\gamma}^{p-2}t_{\delta_2^\gamma}^{-(p-2)}(\gamma_4)$ intersects with m only once since the equations $t_\epsilon^{p-2}t_\delta^{-1}t_{\delta_1^\gamma}^{p-2}t_{\delta_2^\gamma}^{-(p-2)}(\gamma_4) = t_{\delta_1^\gamma}^{p-2}t_\delta^{-1}(\gamma_4) = t_{\delta_1^\gamma}^{p-2}(\gamma_4)$ hold (see the proof of Lemma 4·4), δ_1^γ does not intersect with m and γ_4 in Figure 15 or 22 intersects with m once.

LEMMA 4·4. *The γ curves $(t_{\delta_1^\gamma}^{p-2}(\gamma_1), \gamma_2, t_{\delta_1^\gamma}^{p-2}(\gamma_3), t_{\delta_1^\gamma}^{p-2}(\gamma_4))$ can be obtained by performing the operation $*_\gamma$ for the γ curves of $\mathcal{D}_p$ in Figure 15, where γ_1, γ_3, and δ_1^γ are the curves depicted in Figure 21.*

Proof. We can check from Figure 22 that $t_\delta(\epsilon) = \delta_2^\gamma$ and δ_1^γ in Figure 21 does not intersect with δ_2^γ, δ and ϵ. Thus, for δ_1^γ in Figure 21 and δ_2^γ, δ and ϵ in Figure 22, we have

https://doi.org/10.1017/S0305004125101746 Published online by Cambridge University Press

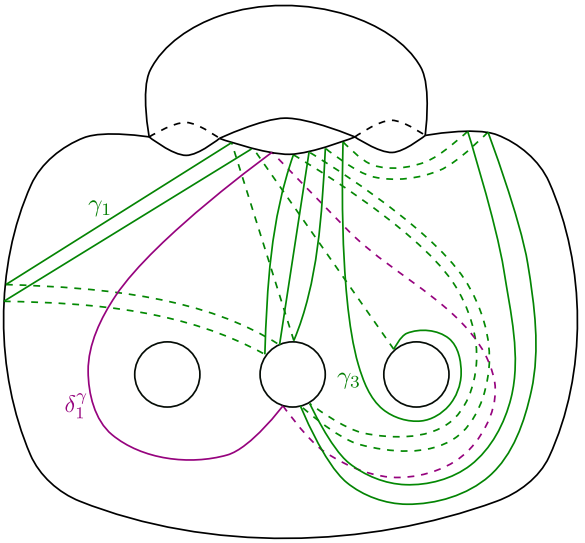


Figure 21. A part of the γ curves obtained by the operation $*_\gamma$ for the γ curves of $\mathcal{D}_p$ (Figure 15).

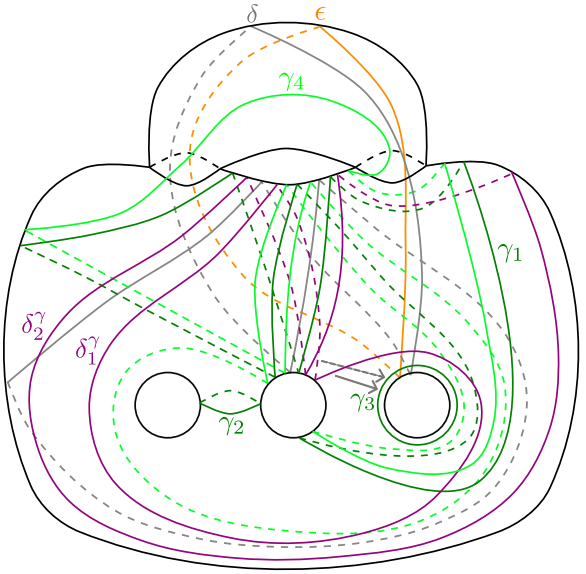


Figure 22. The γ curves of $\mathcal{D}_p$ (Figure 15) and curves δ and ϵ.

$$\begin{aligned} t_\epsilon^{p-2} t_\delta^{-1} t_{\delta_1^\gamma}^{p-2} t_{\delta_2^\gamma}^{-(p-2)} &= t_{\delta_1^\gamma}^{p-2} t_\epsilon^{p-2} t_\delta^{-1} t_{\delta_2^\gamma}^{-(p-2)} \\ &= t_{\delta_1^\gamma}^{p-2} t_\delta^{-1} t_{t_\delta(\epsilon)}^{p-2} t_{\delta_2^\gamma}^{-(p-2)} \\ &= t_{\delta_1^\gamma}^{p-2} t_\delta^{-1} t_{\delta_2^\gamma}^{p-2} t_{\delta_2^\gamma}^{-(p-2)} \\ &= t_{\delta_1^\gamma}^{p-2} t_\delta^{-1}. \end{aligned}$$

https://doi.org/10.1017/S0305004125101746 Published online by Cambridge University Press

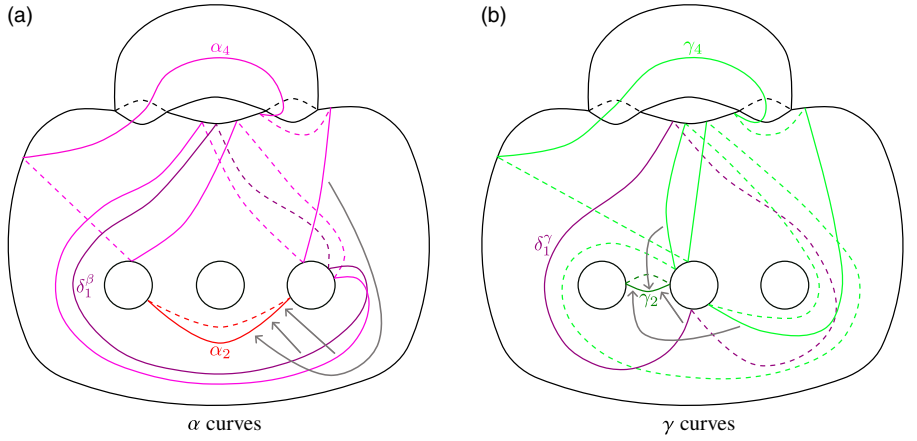


Figure 23. Parts of the α and γ curves obtained by Lemmas 4·2 and 4·3, respectively.

Therefore, the statement for γ_1, γ_2 and γ_4 obviously holds since δ does not intersect with γ_1, γ_2 and γ_4 in Figure 22.

For γ_3, we may consider the following operations: first, perform t_δ^{-1} and $t_{\delta_1^\gamma}^{p-2}$ in order. Then, slide the resulting γ_3 (i.e. $t_{\delta_1^\gamma}^{p-2}t_\delta^{-1}(\gamma_3)$) over $t_{\delta_1^\gamma}^{p-2}(\gamma_4)$ ($=t_{\delta_1^\gamma}^{p-2}t_\delta^{-1}(\gamma_4)$) as indicated in the right-hand side of Figure 17.

We can take the following operations instead of the above operations: first, perform t_δ^{-1}. Then, slide the resulting γ_3 (i.e. $t_\delta^{-1}(\gamma_3)$) over γ_4 ($=t_\delta^{-1}(\gamma_3)$) as indicated in the right-hand side of Figure 17. After that, perform $t_{\delta_1^\gamma}^{p-2}$.

We see that the simple closed curve obtained by handle sliding $t_\delta^{-1}(\gamma_3)$ in Figure 15 (or Figure 22) over γ_4 as indicated in the right-hand side of Figure 17 is γ_3 in Figure 21. This completes the proof.

So, due to Lemmas 4·2, 4·3 and 4·4, we now have the trisection diagram $(\Sigma;\alpha,\beta,\gamma)$ of the Gluck twisted 4-manifold $\Sigma_{S(T(p+1,p))}(S^4)$, where $\alpha=(t_{\delta_1^\beta}^{p-2}t_{\hat\delta}^{-(p-2)}(\alpha_1),\alpha_2,t_{\delta_1^\beta}^{p-2}t_{\tilde\delta}^{p-2}(\alpha_3),t_{\delta_1^\beta}^{p-2}(\alpha_4))$, $\beta=(t_{\delta_1^\beta}^{p-2}(m'),\beta_2,\beta_3,\beta_4=m)$ and $\gamma=(t_{\delta_1^\gamma}^{p-2}(\gamma_1),\gamma_2,t_{\delta_1^\gamma}^{p-2}(\gamma_3),t_{\delta_1^\gamma}^{p-2}(\gamma_4))$ (see Figures 18, 16 and 21, respectively). Recall that $\hat\delta$ and $\tilde\delta$ are the curves depicted in Figure 18. Then, $\beta_4=m$ intersects both α_4 and γ_4 only once. By handle sliding α_4 and γ_4 over α_2 and γ_2, respectively, as indicated in Figure 23, α_4 and γ_4 can be parallel. Moreover, δ_1^β and δ_1^γ can be parallel by the same handle slide (Figure 23). Thus, $t_{\delta_1^\beta}^{p-2}(\alpha_4)$ and $t_{\delta_1^\gamma}^{p-2}(\gamma_4)$ can be parallel (slide other curves if necessary), and we can destabilise the trisection diagram for $t_{\delta_1^\beta}^{p-2}(\alpha_4)$, β_4 and $t_{\delta_1^\gamma}^{p-2}(\gamma_4)$ due to Lemma 3·4. Note that this destabilisation is based on Naylor's method (Lemma 8 in [**18**]). By this destabilisation, we now have the trisection diagram $(\Sigma;\alpha,\beta,\gamma)$ depicted in Figure 24, where $\alpha=(t_{\delta_1^\beta}^{p-2}t_{\hat\delta}^{-(p-2)}(\alpha_1),\alpha_2,t_{\delta_1^\beta}^{p-2}t_{\tilde\delta}^{p-2}(\alpha_3))$, $\beta=(t_{\delta_1^\beta}^{p-2}(\beta_1),\beta_2,\beta_3)$ and $\gamma=(t_{\delta_1^\gamma}^{p-2}(\gamma_1),\gamma_2,t_{\delta_1^\gamma}^{p-2}(\gamma_3))$.

https://doi.org/10.1017/S0305004125101746 Published online by Cambridge University Press

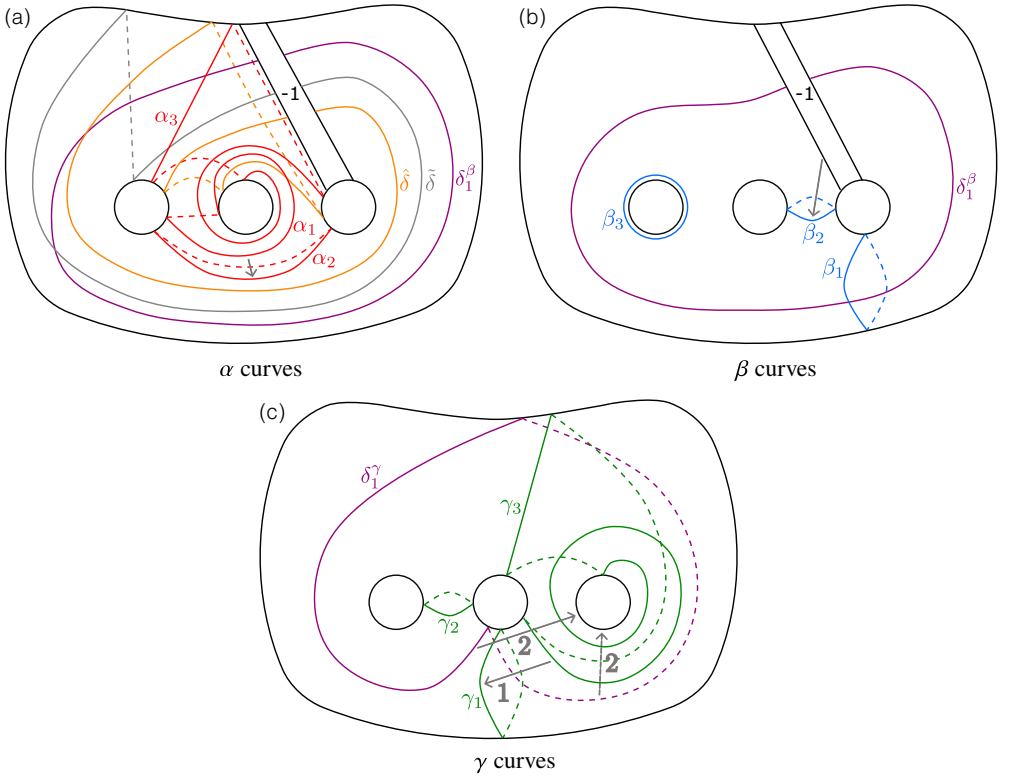


Figure 24. The trisection diagram obtained by the destabilisation in the step 1, where $\alpha = (t_{\delta_1^\beta}^{p-2} t_{\hat{\delta}}^{-(p-2)}(\alpha_1), \alpha_2, t_{\delta_1^\beta}^{p-2} t_{\tilde{\delta}}^{p-2}(\alpha_3))$, $\beta = (t_{\delta_1^\beta}^{p-2}(\beta_1), \beta_2, \beta_3)$ and $\gamma = (t_{\delta_1^\gamma}^{p-2}(\gamma_1), \gamma_2, t_{\delta_1^\gamma}^{p-2}(\gamma_3))$.

Step 2. Reduce the destabilised trisection diagram to the stabilisation of the genus-0 trisection diagram.

We make some preparations to adapt the seesaw lemma (Lemma 4·6). In Figure 24, slide γ_3 over γ_1 as indicated in Figure 24 (labeled 1), perform t_{β_2} for the entire diagram and slide α_1 over α_2 as indicated in Figure 24. Then, the trisection diagram $(\Sigma; \alpha, \beta, \gamma)$ depicted in Figure 25, where $\alpha = (t_{\delta_1^\beta}^{p-2} t_{\hat{\delta}}^{-(p-2)}(\alpha_1), \alpha_2, t_{\delta_1^\beta}^{p-2} t_{\tilde{\delta}}^{p-2}(\alpha_3))$, $\beta = (t_{\delta_1^\gamma}^{p-2}(\beta_1), \beta_2, \beta_3)$ and $\gamma = (t_{\delta_1^\gamma}^{p-2}(\gamma_1), \gamma_2, t_{\delta_1^\gamma}^{p-2}(\gamma_3))$, can be obtained. Note that we here slide δ_1^β and δ_1^γ over β_2 and the new γ_3 (i.e. γ_3 in Figure 25), respectively, as indicated in Figure 24 (Lemma 3·4). Let $g(\gamma)$ denotes $(g(\gamma_1), g(\gamma_2), g(\gamma_3))$ for a surface diffeomorphism g and a collection of simple closed curves $\gamma = (\gamma_1, \gamma_2, \gamma_3)$.

LEMMA 4·5. *The trisection diagram* $(\Sigma; \alpha, \beta, \gamma)$ *depicted in Figure* 26, *where* $\alpha = (\alpha_1, \alpha_2, \alpha_3)$, $\beta = (\beta_1, \beta_2, \beta_3)$ *and* $\gamma = t_{\tilde{\delta}}^{-(p-2)} t_{\hat{\delta}}^{p-2} t_{\delta_1^\beta}^{-(p-2)} t_{\delta_1^\gamma}^{p-2}(\gamma_1, \gamma_2, \gamma_3)$, *can be obtained from the trisection diagram depicted in Figure* 25.

Proof. By performing $t_{\tilde{\delta}}^{-(p-2)} t_{\hat{\delta}}^{p-2} t_{\delta_1^\beta}^{-(p-2)}$ for the trisection diagram depicted in Figure 25, we have the trisection diagram

https://doi.org/10.1017/S0305004125101746 Published online by Cambridge University Press

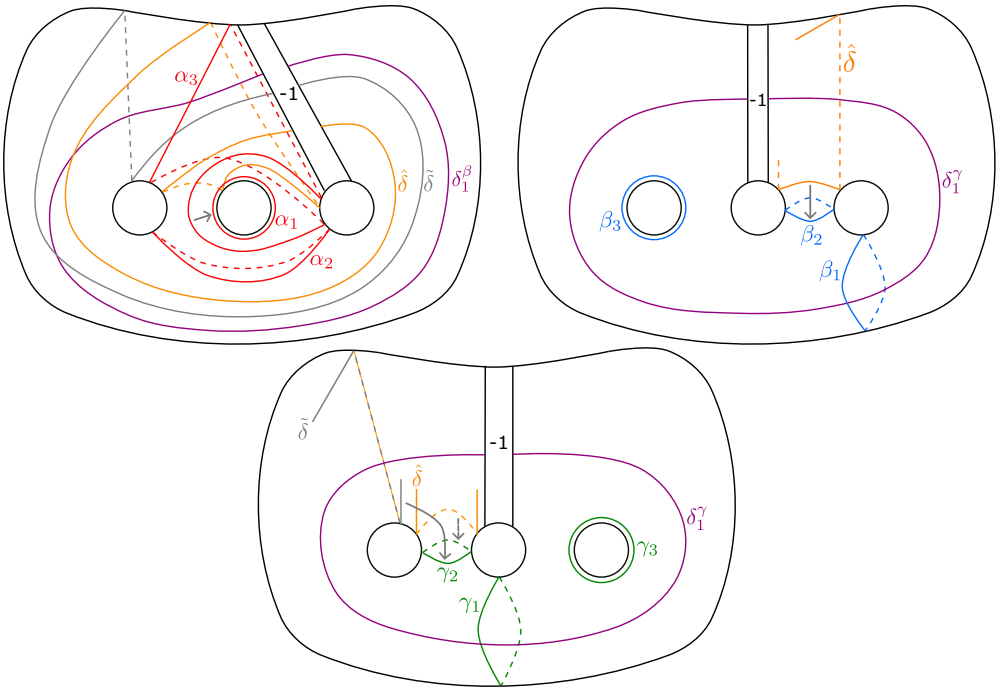


Figure 25. The trisection diagram obtained from Figure 24 after some handle slides and Dehn twists, where $\alpha = (t_{\delta_1^\beta}^{p-2} t_{\hat{\delta}}^{-(p-2)}(\alpha_1), \alpha_2, t_{\delta_1^\beta}^{p-2} t_{\tilde{\delta}}^{p-2}(\alpha_3))$, $\beta = (t_{\delta_1^\gamma}^{p-2}(\beta_1), \beta_2, \beta_3)$ and $\gamma = (t_{\delta_1^\gamma}^{p-2}(\gamma_1), \gamma_2, t_{\delta_1^\gamma}^{p-2}(\gamma_3))$. In the figure of the β curves, a part of $\hat{\delta}$ in the figure of the α curves is depicted. In the figure of the γ curves, parts of $\tilde{\delta}$ and $\hat{\delta}$ in the figure of the α curves are depicted.

$$(\Sigma; \alpha, t_{\tilde{\delta}}^{-(p-2)} t_{\hat{\delta}}^{p-2} t_{\delta_1^\beta}^{-(p-2)} t_{\delta_1^\gamma}^{p-2}(\beta), t_{\tilde{\delta}}^{-(p-2)} t_{\hat{\delta}}^{p-2} t_{\delta_1^\beta}^{-(p-2)} t_{\delta_1^\gamma}^{p-2}(\gamma)),$$

where $\alpha = (\alpha_1, \alpha_2, \alpha_3)$, $\beta = (\beta_1, \beta_2, \beta_3)$ and $\gamma = (\gamma_1, \gamma_2, \gamma_3)$ in Figure 25 and $\tilde{\delta}$, $\hat{\delta}$, δ_1^β and δ_1^γ are the curves in Figure 25. By sliding α_3 over α_1 as indicated in Figure 25, we have the α curves in Figure 26. By sliding $\hat{\delta}$ and δ_1^β over β_2 as indicated in Figures 25 and 24 (*b*), respectively, $\hat{\delta}$ and δ_1^β can be parallel to $\tilde{\delta}$ and δ_1^γ, respectively. Thus, $t_{\tilde{\delta}}^{-(p-2)} t_{\hat{\delta}}^{p-2} t_{\delta_1^\beta}^{-(p-2)} t_{\delta_1^\gamma}^{p-2}(\beta_1, \beta_2, \beta_3)$ can be regarded as the β curves $(\beta_1, \beta_2, \beta_3)$ in Figure 26 due to Lemma 3·4. In the γ curves, $\tilde{\delta}$ and $\hat{\delta}$ in Figure 26 is obtained by sliding $\tilde{\delta}$ and $\hat{\delta}$ in Figure 25 over γ_2 as indicated in Figure 25 (Lemma 3·4). This completes the proof.

In Figure 26, $\hat{\delta} = t_m^{-1}(\delta_1^\beta)$ and $\tilde{\delta} = t_m^{-1}(\delta_1^\gamma)$. Thus, $t_{\tilde{\delta}}^{-(p-2)} t_{\hat{\delta}}^{p-2} t_{\delta_1^\beta}^{-(p-2)} t_{\delta_1^\gamma}^{p-2} = t_m^{-1} t_{f_{p-2}(m)}$, where $f_{p-2} = t_{\delta_1^\beta}^{-(p-2)} t_{\delta_1^\gamma}^{p-2} = (t_{\delta_1^\beta}^{-1} t_{\delta_1^\gamma})^{p-2}$. Here, the trisection diagram $(\Sigma; \alpha, \beta, t_m^{-1} t_{f_{p-2}(m)}(\gamma))$ is obtained from Lemma 4·5. Then, $(\Sigma; \alpha, \beta, t_{f_{p-2}(m)}(\gamma))$ is obtained by performing t_m for the trisection diagram $(\Sigma; \alpha, \beta, t_m^{-1} t_{f_{p-2}(m)}(\gamma))$. For this trisection diagram $(\Sigma; \alpha, \beta, t_{f_{p-2}(m)}(\gamma))$, the following key lemma holds, which we call the seesaw lemma.

https://doi.org/10.1017/S0305004125101746 Published online by Cambridge University Press

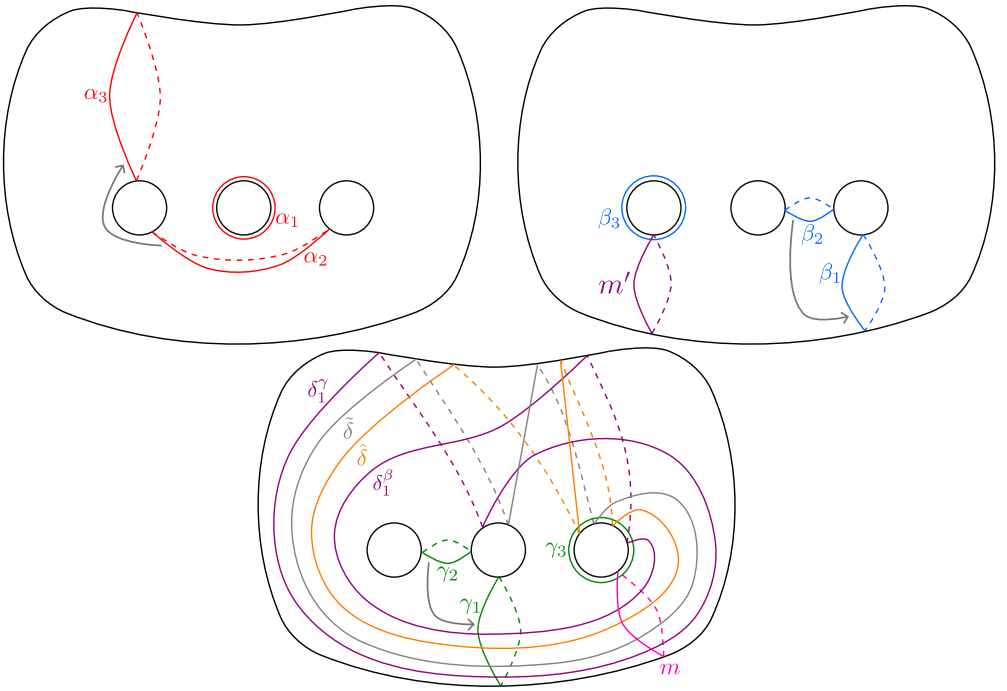


Figure 26. The trisection diagram obtained in Lemma 4·4, where $\alpha = (\alpha_1, \alpha_2, \alpha_3)$, $\beta = (\beta_1, \beta_2, \beta_3)$, $\gamma = t_{f_{p-2}(m)}(\gamma_1, \gamma_2, \gamma_3)$ and $f_{p-2} = t_{\delta_1^\beta}^{-(p-2)} t_{\delta_1^\gamma}^{p-2} = (t_{\delta_1^\beta}^{-1} t_{\delta_1^\gamma})^{p-2}$.

LEMMA 4·6 (The seesaw lemma). *Let* $\alpha = (\alpha_1, \alpha_2, \alpha_3)$, $\beta = (\beta_1, \beta_2, \beta_3)$ *and* $\gamma = (\gamma_1, \gamma_2, \gamma_3)$ *in Figure 26. Then, the trisection diagrams* $(\Sigma; \alpha, \beta, t_{f_{p-2}(m)}(\gamma))$ *and* $(\Sigma; \alpha, t_{m'}(\beta), t_{f_{p-3}(m)}(\gamma))$ *are related by surface diffeomorphisms and handle slides.*

Proof. We focus on the simple closed curve $f_{p-2}(m)$. By performing $t^{-1}_{f_{p-2}(m)}$ for $(\Sigma; \alpha, \beta, t_{f_{p-2}(m)}(\gamma))$, $(\Sigma; t^{-1}_{f_{p-2}(m)}(\alpha), t^{-1}_{f_{p-2}(m)}(\beta), \gamma)$ is obtained. Then, since $f_{p-2}(m)$ can be parallel to m by sliding $f_{p-2}(m)$ over β_2 $p-2$ times as indicated in Figure 24 (*b*), $(\Sigma; t^{-1}_{f_{p-2}(m)}(\alpha), \beta, \gamma)$ is obtained from $(\Sigma; t^{-1}_{f_{p-2}(m)}(\alpha), t^{-1}_{f_{p-2}(m)}(\beta), \gamma)$ by the handle slides due to Lemma 3·4. In the α curves, $f_{p-2}(m')$ is obtained by sliding $f_{p-2}(m)$ over α_2 as indicated in Figure 23 (*a*). Thus, $(\Sigma; t^{-1}_{f_{p-2}(m')}(\alpha), \beta, \gamma)$ is obtained from $(\Sigma; t^{-1}_{f_{p-2}(m)}(\alpha), \beta, \gamma)$ by the handle slide due to Lemma 3·4. By performing $t_{f_{p-2}(m')}$ for $(\Sigma; t^{-1}_{f_{p-2}(m')}(\alpha), \beta, \gamma)$, $(\Sigma; \alpha, t_{f_{p-2}(m')}(\beta), t_{f_{p-2}(m')}(\gamma))$ is obtained. In the β curves, since $f_{p-2}(m')$ can be parallel to m' by sliding $f_{p-2}(m')$ over β_2 $p-2$ times as indicated in Figure 25, $(\Sigma; \alpha, t_{m'}(\beta), t_{f_{p-2}(m')}(\gamma))$ is obtained from $(\Sigma; \alpha, t_{f_{p-2}(m')}(\beta), t_{f_{p-2}(m')}(\gamma))$ by the handle slides due to Lemma 3·4. Moreover, in the γ curves, $f_{p-2}(m')$ can be parallel to $f_{p-3}(m)$ by sliding $f_{p-2}(m')$ over γ_2 as indicated in $\hat{\delta}$ of Figure 25 since $f_1(m')$ can be parallel to m by sliding $f_1(m')$ over γ_2 as indicated in $\hat{\delta}$ of Figure 25. Thus, $(\Sigma; \alpha, t_{m'}(\beta), t_{f_{p-3}(m)}(\gamma))$ is obtained from $(\Sigma; \alpha, t_{m'}(\beta), t_{f_{p-2}(m')}(\gamma))$ by the handle slide due to Lemma 3·4. This completes the proof.

https://doi.org/10.1017/S0305004125101746 Published online by Cambridge University Press

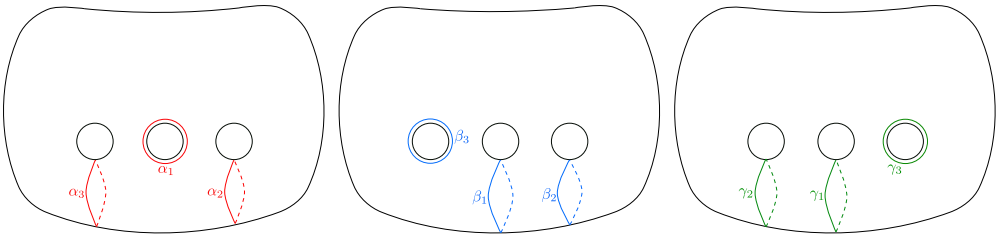


Figure 27. The stabilisation of the genus-0 trisection diagram of S^4.

We can use the seesaw lemma iterately since in the proof of the seesaw lemma, we only consider handle sliding $f_i(m)$ over α_2, β_2 and γ_2. Using the seesaw lemma $p-2$ times for $(\Sigma;\alpha,\beta,t_{f_{p-2}(m)}(\gamma))$, we have $(\Sigma;\alpha,t_{m'}^{p-2}(\beta),t_m(\gamma))$ (Figure 26). By performing $t_{m'}^{-(p-2)}t_m^{-1}$ for this trisection diagram and sliding α_2 over α_3, β_2 over β_1 and γ_2 over γ_1 as indicated in Figure 26, we have the trisection diagram $(\Sigma;\alpha,\beta,\gamma)$ depicted in Figure 27, which is just the stabilisation of the genus-0 trisection diagram of S^4. This completes the proof of Theorem 4·1.

5. *Further remarks and questions*

In [13], Kim and Miller introduced a new technique called a *boundary-stabilisation* to construct a relative trisection of the complement of a surface-knot and gave an algorithm for constructing its diagram. Then, they submitted the following question.

Question 5·1 [13, question 6.2]. Let S be a P^2-knot in S^4 and $\Sigma_S(S^4)$ the Price twisted homotopy 4-sphere. We consider the case that $\Sigma_S(S^4)$ is diffeomorphic to S^4. Is a trisection diagram of $\Sigma_S(S^4)$ obtained from the algorithm standard?

Note that a *P^2-knot* is an embedded real projective plane and the *Price twist* is a cutting and pasting operation along a P^2-knot. The Price twist for S^4 on a P^2-knot S provides us with at most three 4-manifolds up to diffeomorphism, namely, S^4, a homotopy 4-sphere $\Sigma_S(S^4)$ and $\tau_S(S^4)$ which is not simply-connected.

It is known that for the unknotted P^2-knot P and any 2-knot K, $\Sigma_{P\#K}(S^4)$ is diffeomorphic to the Gluck twisted 4-manifold on K [12]. Naylor [18] showed that the trisection diagram in Question 5·1 is related to the trisection diagram of the Gluck twisted 4-manifold on K given in [6] without stabilisations. Therefore, Theorem 4·1 also answers affirmatively in the case of $S=P\#S(T(p+1,p))$ (and the doubly-pointed trisection diagram). Note that a P^2-knot $P\#K$ is called of *Kinoshita type*. It is not yet known whether any P^2-knot is of Kinoshita type.

The author and Ogawa [11] explicitly depicted the trisection diagram appearing in Question 1·1 in the case of the spun $(2n+1,2)$-torus knot, where $n\geq 1$, and showed that the trisection diagram is standard when $n=1$. (Recall that this result corresponds to the case of $p=2$ in this paper.) However, we have yet to detect whether the trisection diagram is standard when $n\geq 2$. So, we submit the following question:

Question 5·2. Is the trisection diagram of $\Sigma_{S(T(2n+1,2))}(S^4)$ in [11] standard when $n\geq 2$?

https://doi.org/10.1017/S0305004125101746 Published online by Cambridge University Press

Acknowledgement. The author would like to express sincere gratitude to his supervisor, Hisaaki Endo, for his helpful comments. He would also like to thank the anonymous referee for their many valuable and insightful comments. This work was partially supported by Grant-in-Aid for JSPS Research Fellow from JSPS KAKENHI Grant Number JP23KJ0888.

REFERENCES

[1] N. A. CASTRO. Relative trisections of smooth 4-manifolds with boundary. PhD. thesis. University of Georgia (2016).
[2] N. A. CASTRO, D. T. GAY and J. PINZÓN-CAICEDO. Diagrams for relative trisections. *Pacific J. Math.* **294**(2) (2018), 275–305.
[3] B. FARB and D. MARGALIT. *A primer on mapping class groups*. Princeton Math. Ser. vol. 49 (Princeton University Press, Princeton, NJ, 2011).
[4] M. H. FREEDMAN. The topology of four-dimensional manifolds. *J. Differential Geom.* **17** (1982), 357–453.
[5] D. GAY and R. KIRBY. Trisecting 4-manifolds. *Geom. Topol.* **20**(6) (2016), 3097–3132.
[6] D. GAY and J. MEIER. Doubly pointed trisection diagrams and surgery on 2-knots. *Math. Proc. Camb. Phil. Soc.* **172**(1) (2022), 163–195.
[7] H. GLUCK. The embedding of two-spheres in the four-sphere. *Trans. Amer. Math. Soc.* **104** (1962), 308–333.
[8] C. M. GORDON. Knots in the 4-sphere. *Comment. Math. Helv.* **51** December (1976) 585–596.
[9] G. ISLAMBOULI. Nielsen equivalence and trisections. *Geom. Dedicata* **214** (2021), 303–317.
[10] T. ISOSHIMA. Trisections obtained by trivially regluing surface-knots. *Geom. Dedicata* **218**(3) (2021), Paper No. 71, 19.
[11] T. ISOSHIMA and M. OGAWA. Trisections induced by the Gluck surgery along certain spun knots. *J. Knot Theory Ramifications* **33**(3) (2024), Paper No. 2450007.
[12] A. KATANAGA, O. SAEKI, M. TERAGAITO and Y. YAMADA. Gluck surgery along a 2-sphere in a 4-manifold is realized by surgery along a projective plane. *Michigan Math. J.* **46**(3) (1999), 555–571.
[13] S. KIM and M. MILLER. Trisections of surface complements and the Price twist. *Algebr. Geom. Topol.* **20**(1) (2020), 343–373.
[14] J. MEIER. Trisections and spun four-manifolds. *Math. Res. Lett.* **25**(5) (2018), 1497–1524.
[15] J. MEIER, T. SCHIRMER and A. ZUPAN. Classification of trisections and the generalized property R conjecture. *Proc. Amer. Math. Soc.* **144**(11) (2016), 4983–4997.
[16] J. MEIER and A. ZUPAN. Bridge trisections of knotted surfaces in S^4. *Trans. Amer. Math. Soc.* **369**(10) (2017), 7343–7386.
[17] J. MEIER and A. ZUPAN. Bridge trisections of knotted surfaces in 4-manifolds. *Proc. Natl. Acad. Sci. USA* **115**(43) (2018), 10880–10886.
[18] P. NAYLOR. Trisection diagrams and twists of 4-manifolds. *C. R. Math. Acad. Sci. Paris* **360** (2022), 845–866.
[19] P. ORDING. Constructing doubly-pointed Heegaard diagrams compatible with (1,1) knots. *J. Knot Theory Ramifications* **22**(11) (2013), 1350071, 26.

https://doi.org/10.1017/S0305004125101746 Published online by Cambridge University Press